Power-Optimal Guidance for Planar Space Solar Power Satellites

Michael A. Marshall*
California Institute of Technology, Pasadena, California, 91125

Ashish Goel†
Jet Propulsion Laboratory, Pasadena, California, 91109

Sergio Pellegrino‡
California Institute of Technology, Pasadena, California, 91125

This paper presents power-optimal guidance for a planar space solar power satellite (SSPS). Power-optimal guidance is the attitude trajectory that maximizes the solar power transmitted by the SSPS. Maximizing the transmitted power simultaneously maximizes the cumulative energy delivered to the receiving station. Planarity couples the orientations of the SSPS's photovoltaic and antennas surfaces. Hence, the transmitted power only depends on the relative geometry between the SSPS, Sun, and receiving station. The orientation that maximizes power transfer changes as this relative geometry changes. Both single and dual-sided SSPS architectures are considered. A single-sided SSPS has one photovoltaic surface and one antenna surface. A dual-sided SSPS is a single-sided SSPS with at least one additional photovoltaic or antenna surface. Geometric arguments show that a dual-sided SSPS has superior performance to a single-sided SSPS. Power-optimal guidance is then determined numerically for several examples, including for an SSPS in GEO. These examples emphasize important solution properties, including the need for large slew maneuvers, and show that even though system efficiency decreases as orbit altitude decreases, reduced path losses actually increase the total amount of received energy per unit aperture area. This has significant system implications for future space solar power missions.

Nomenclature

A	=	area - m^2
AF(ϕ)	=	phased array factor

---

*Graduate Research Assistant, Graduate Aerospace Laboratories, 1200 E. California Blvd., Mail Code 105-50; mmarshall@caltech.edu.

†Postdoctoral Researcher, 4800 Oak Grove Dr.; ashish.goel@jpl.nasa.gov.

‡Joyce and Kent Kresa Professor of Aerospace and Civil Engineering, Jet Propulsion Laboratory Senior Research Scientist; Co-Director, Space-Based Solar Power Project, Graduate Aerospace Laboratories, 1200 E. California Blvd., Mail Code 105-50; sergiop@caltech.edu. AIAA Fellow.

$\mathcal{D}$	=	domain, subset of $\mathbb{R}$
G	=	geometric efficiency
$\overline{G}$	=	average geometric efficiency
i	=	integer
E	=	energy per unit aperture area - J/m^2
J^*	=	value of objective function at optimum
k	=	time step k
N	=	total number of time steps
$\mathbf{\hat{n}}$	=	outward unit normal vector
n	=	mean motion - rad s^{-1}
P	=	power - W
$\mathrm{PV}(\beta)$	=	photovoltaic efficiency function
$\mathbf{R}$	=	receiving station position - m
$R_\oplus$	=	mean Earth radius, - m
$\mathrm{RF}(\phi)$	=	antenna efficiency function
$\mathbf{r}$	=	spacecraft position - m
$\mathbf{\hat{s}}$	=	sun vector
t	=	time variable - s
W	=	power per unit aperture area - W/m^2
$\overline{W}$	=	average power per unit aperture area - W/m^2
W_{SF}	=	incident solar flux - 1,361 W/m^2
$\{\mathbf{\hat{X}}, \mathbf{\hat{Y}}, \mathbf{\hat{Z}}\}$	=	basis vectors for Earth-Centered Inertial (ECI) reference frame
β	=	sun angle - rad or °
β^*	=	optimal value of sun angle - rad or °
γ	=	$\theta + \delta' - \pi/2$ - rad or °
δ	=	elevation angle in $[0°, 90°]$ - rad or °
δ'	=	elevation angle in $[0°, 180°]$ - rad or °
$\eta_{\mathrm{PV}}, \eta_{\mathrm{DC\text{-}RF}}, \eta_{\mathrm{Tx}}, \eta_{\mathrm{ML}}$	=	system efficiencies
θ	=	angular position of receiving station - rad or °
λ	=	wavelength - m
ν	=	orbit true anomaly - rad or °
$\boldsymbol{\rho}$	=	slant vector - m

ρ	=	slant range - m
ϕ	=	squint angle - rad or $^\circ$
$\omega_\oplus$	=	rotation rate of Earth about its axis - $\mathrm{rad\,s^{-1}}$
$\mathbb{1}$	=	indicator function
Subscripts		
f	=	final condition (e.g. t is equal to t_f)
PV	=	photovoltaic surface
r	=	receiver
RF	=	radio-frequency surface
t	=	transmitter
0	=	initial condition (e.g. t is equal to t_0)

I. Introduction

SPACE solar power involves collecting solar power in space and wirelessly transmitting it to Earth. Compared to terrestrial solar power, space solar has several benefits. For one, it decouples solar power collection from terrestrial weather and diurnal and seasonal cycles. Additionally, space solar can provide power to virtually any location on Earth at any time, irrespective of latitude and weather conditions.

Isaac Asimov first mentioned the idea of space solar in a science fiction magazine in 1941 [1]. However, another two decades passed before P. E. Glaser proposed the first technical concept for a space solar power satellite (SSPS) [2]. In the years since, researchers have proposed a variety of SSPS concepts [3–7], all of which are essentially variations of the original concept proposed by Glaser. In particular, these "classical" SSPS concepts feature large photovoltaic (PV) arrays that convert solar power to direct current (DC) power, a DC to radio frequency (RF) converter, and one or more antennas for beaming RF power to Earth. Moreover, these concepts typically include either *mechanically steerable* solar arrays or antennas that decouple the problems of antenna steering and sun pointing.

However, aggressive new structural concepts characterized by extremely low areal mass densities (on the order of $1\,\mathrm{kg\,m^{-2}}$ or less) are enabling the development of new ultralight, planar SSPS concepts [8]. These concepts replace a monolithic SSPS with formations of smaller SSPSs and replace complicated mechanical subsystems with lightweight, planar elements consisting of integrated PV surfaces, DC to microwave converters, and microwave patch antennas [8–10].

Whereas classical SSPS concepts typically require multiple launches and in-space assembly to realize a functional system (e.g. [5, 11]), a planar spacecraft architecture is advantageous because it enables multiple lightweight, packageable, and self-deployable spacecraft to launch on a single existing rocket [8]. This greatly reduces both system
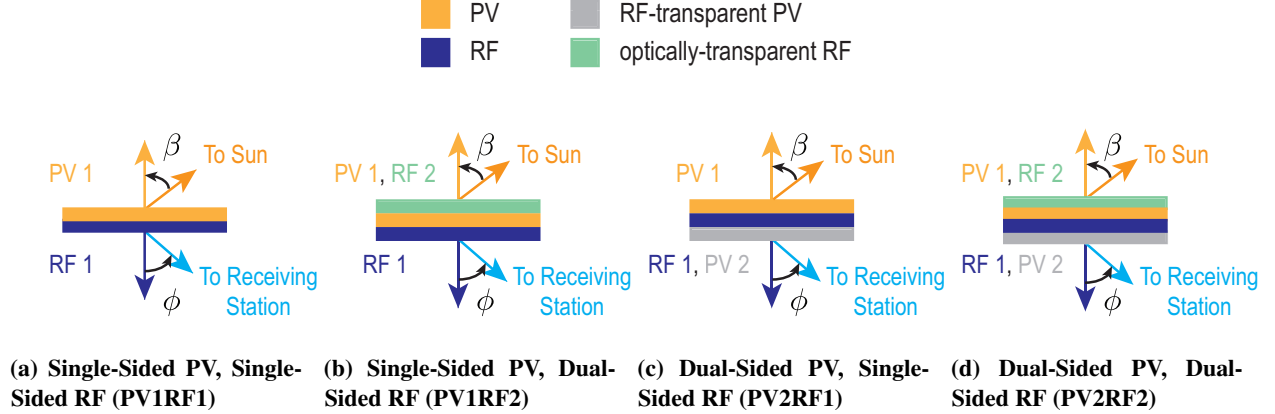
cost and complexity and simplifies the spacecraft structural architecture. A key challenge of this approach is that orienting the PV surface towards the Sun and steering the RF beam towards the Earth are intrinsically coupled, i.e., reorienting the PV surface reorients the RF surface and vice versa. This critical difference between classical and planar SSPS architectures motivates the power-optimal guidance problem considered in this paper.

The power-optimal guidance problem defines the orientation of an SSPS that maximizes the power transmitted to Earth. Power-optimal guidance is just one of the many guidance, navigation, and control (GNC) challenges associated with flying a planar SSPS. Various authors have studied GNC challenges for classical SSPS concepts (e.g. [7, 12–15]). However, aside from the preliminary studies for geostationary SSPS concepts presented in [16] and [17], the power-optimal guidance problem and the related GNC problems for a planar SSPS are to our knowledge largely unexplored in the literature. To that end, this paper expands on the recent results in [16] by considering non-geostationary orbits and additional SSPS architectures. Dynamics and perturbations are intentionally neglected to focus exclusively on ideal SSPS mission geometry. The goal is to provide insights into the power-optimal guidance problem that establish a framework for designing solutions for practical SSPS missions.

The baseline SSPS architecture considered in this paper consists of two primary layers. The top layer contains PV cells that convert incident sunlight into direct current (DC) electrical power. This DC electrical power is then converted to RF power by the integrated circuits (ICs) located on the underside of the top layer. The bottom layer consists of small patch antennas that radiate the collected power towards Earth. These patch antennas rely on precision timing circuits to operate as a phased array with beam-forming and beam-steering capabilities. Throughout this paper, this baseline architecture is referred to as single-sided PV, single-sided RF (PV1RF1).

Several "dual-sided" variations of this baseline architecture are also considered. In this context, dual-sided refers to an SSPS with at least two PV surfaces or two RF surfaces. A dual-sided SSPS is constructed by adding a layer of optically-transparent antennas or RF-transparent PV cells to the top or bottom layers of the baseline architecture. The dual-sided modifications significantly improve the performance of the SSPS. The addition of a layer of optically-transparent antennas to the baseline architecture is referred to as single-sided PV, dual-sided RF (PV1RF2). Similarly, the addition of RF-transparent PV cells is referred to as dual-sided PV, single-sided RF (PV2RF1). The addition of both optically-transparent antennas and RF-transparent PV cells is termed dual-sided PV, dual-sided RF (PV2RF2). Note that for any dual-sided SSPS, only a single PV surface and a single RF surface operate at any given time. The four SSPS architectures considered in this paper are depicted in Fig. 1 where β and ϕ denote the orientations of the top PV surface relative to the Sun and the bottom RF surface relative to the receiving station. β and ϕ are referred to as the sun and squint angles, respectively.

This paper is organized as follows: Sec. II formulates the power-optimal guidance problem. Next, Sec. III uses geometric arguments to derive an inequality that relates the power transmitted by each SSPS architecture from Fig. 1. Several representative solutions to the power-optimal guidance problem are presented in Sec. IV, followed by a discussion

(a) Single-Sided PV, Single-Sided RF (PV1RF1) **(b) Single-Sided PV, Dual-Sided RF (PV1RF2)** **(c) Dual-Sided PV, Single-Sided RF (PV2RF1)** **(d) Dual-Sided PV, Dual-Sided RF (PV2RF2)**

Fig. 1   Baseline SSPS architecture and dual-sided variations.

of system performance metrics and their ramifications in Sec. V. Finally, the paper's conclusions are summarized in Sec. VI.

II. Problem Formulation

This section formulates the power-optimal guidance problem for a planar SSPS. This problem defines the orientation over one or more orbits that maximizes the total power transmitted to a receiving station on Earth. Power-optimality only depends on the relative geometry between the SSPS, the Sun, and the receiving station. The power-optimal guidance problem is defined for an SSPS in an arbitrary orbit transmitting to an arbitrarily located receiving station, and it is subsequently restricted to the special case of an SSPS in a circular, equatorial orbit transmitting to an equatorial receiving station.

A. General Formulation

Figure 2 depicts the problem geometry used to formulate the power-optimal guidance problem. An Earth-Centered Inertial (ECI) reference frame is defined to locate the SSPS and receiving station. The ECI frame is inertially-fixed with its origin at the center of the Earth and is defined by the basis vectors $\{\hat{\mathbf{X}}, \hat{\mathbf{Y}}, \hat{\mathbf{Z}}\}$. $\hat{\mathbf{X}}$ points towards the vernal equinox, $\hat{\mathbf{Z}}$ points towards the North Pole, and $\hat{\mathbf{Y}} = \hat{\mathbf{Z}} \times \hat{\mathbf{X}}$. $\hat{\mathbf{X}}$ and $\hat{\mathbf{Y}}$ define Earth's equatorial plane. $\hat{\mathbf{s}}$ is the time-varying vector from the center of the Earth to the center of the Sun, also referred to as the "sun vector". At the vernal equinox, $\hat{\mathbf{s}} = \hat{\mathbf{X}}$.

The transmitted power only depends on the orientation of the SSPS relative to both the Sun and the receiving station. The orientation of a planar SSPS can be defined by either of its two outward normal vectors, $\hat{\mathbf{n}}_{PV1}$ and $\hat{\mathbf{n}}_{RF1}$, so long as both the PV and RF surfaces have no radial (azimuthal) dependencies. $\hat{\mathbf{n}}_{PV1}$ and $\hat{\mathbf{n}}_{RF1}$ are the outward normal vectors from the SSPS's PV 1 and RF 1 surfaces, respectively, and satisfy the identity $\hat{\mathbf{n}}_{PV1} = -\hat{\mathbf{n}}_{RF1}$. The sun angle, β, is
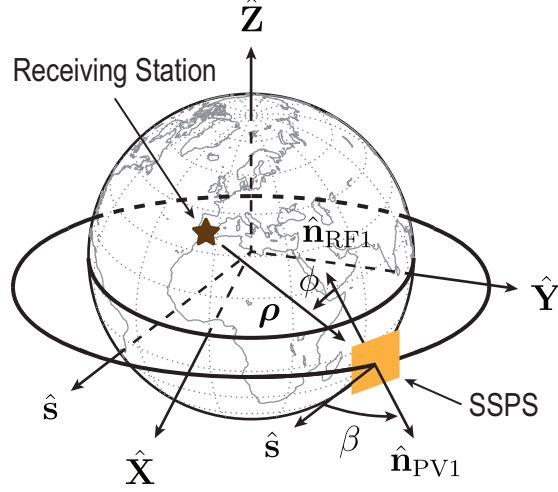
Fig. 2   Earth-Centered Inertial (ECI) reference frame definition and problem geometry. Even though this figure depicts an equatorial orbit, this geometric framework is applicable for an SSPS in any orbit.

defined as the angle between $\hat{\mathbf{n}}_{PV1}$ and the sun vector, i.e.,

$$\cos(\beta) = \hat{\mathbf{n}}_{PV1} \cdot \hat{\mathbf{s}} \tag{1}$$

Equation (1) assumes that incident sunlight is collimated. Similarly, the squint angle, ϕ, is defined as the angle between $\hat{\mathbf{n}}_{RF1}$ and the slant vector, i.e.,

$$\cos(\phi) = -\frac{\hat{\mathbf{n}}_{RF1} \cdot \boldsymbol{\rho}}{\rho} \tag{2}$$

where $\boldsymbol{\rho} = \mathbf{r} - \mathbf{R}$ is the slant vector pointing from the receiving station to the SSPS, $\rho = ||\boldsymbol{\rho}||$ is the Euclidean norm of $\boldsymbol{\rho}$, and $\mathbf{r}$ and $\mathbf{R}$ denote the positions of the SSPS and receiving station, respectively. The sun and squint angles are assumed to be in $[-180°, 180°)$. Equations (1) and (2) are the orbit-attitude coupling relations for a planar SSPS. Combining Eqs. (1) and (2) results in a single transcendental equation relating the sun and squint angles to the spacecraft's attitude.

Power transmission requires the SSPS to be above the horizon relative to the receiving station. This only occurs when the elevation angle, δ, of the SSPS relative to the receiving station exceeds some minimum elevation angle. Using the identity $\cos(\pi/2 - \delta) = \sin(\delta)$ results in the following expression for the elevation angle of the SSPS:

$$\sin(\delta) = \frac{\mathbf{R} \cdot \boldsymbol{\rho}}{R_{\oplus}\, \rho} \tag{3}$$

where δ is defined relative to the local horizon at the receiving station and $R_{\oplus} = ||\mathbf{R}||$. The SSPS is assumed to be able to transmit to the receiving station for elevation angles that exceed 5° above the horizon, i.e, for $\delta \in [5°, 90°]$.

Power transmission also requires the SSPS to be in direct sunlight, i.e., not in eclipse. Eclipse periods are modeled as a binary on/off using the conical projection method described in [18]. Penumbral shadowing is ignored, meaning

the spacecraft is either in eclipse and sees no sunlight or vice versa. Penumbral shadowing can be modeled as an orbit-dependent scale factor that attenuates the incident solar flux (e.g. [19–21]). However, as shown in Section II.D, the orientation that maximizes power transfer only depends on the problem geometry, not the magnitude of the solar insolation. As a result, neglecting penumbral shadowing does not affect the orientation that maximizes power transfer.

B. Formulation for Circular, Equatorial Orbits and Equatorial Receiving Stations

The formulation from Sec. II.A is now restricted to the special case of an SSPS in a circular, equatorial orbit transmitting to an equatorial receiving station at the vernal equinox. The power-optimal guidance problem for this special case is referred to as the *restricted power-optimal guidance problem*. Due to its utility for approximating possible mission scenarios, this paper focuses on the restricted power-optimal guidance problem.

These restrictions are made for several reasons. First, effects due to precession of the orbit plane are not important in a circular, equatorial orbit. An SSPS in an inclined orbit requires stationkeeping to counteract precession and maintain consistent levels of coverage over a receiving station. Next, an equatorial orbit enables the SSPS to provide power to a receiving station on either side of the equator at any point in its orbit. Finally, only considering an equatorial receiving station simplifies the problem geometry in order to provide useful insights into power-optimal guidance. However, a practical system would likely have a receiving station at a middle latitude due to the distribution of Earth's population.

It is also assumed that the Earth's position is fixed at the vernal equinox to facilitate the development of useful analytical results. Fixing the Earth-Sun geometry is a reasonable approximation for short durations of time relative to Earth's orbit period about the Sun, like the sidereal day used in the remainder of this paper. As previously noted, $\hat{s} = \hat{X}$ at the equinox, from which it follows that Earth's equatorial plane is coplanar with a great circle of the Sun. This reduces the general three-dimensional problem to a planar, two-dimensional problem. As a result, Earth's axial tilt does not affect the transmitted power and the sun vector is inertially-fixed, i.e., β is defined relative to an inertial reference. Because the sun vector lies in Earth's equatorial plane, only a single rotational degree of freedom is required to uniquely define the orientation of the SSPS. Hence, either β or ϕ can uniquely define this orientation, but β is chosen in subsequent developments for mathematical convenience. Note that the equinox coincides with the worst-case eclipse conditions for an equatorial orbit and that a geostationary satellite experiences eclipsing at the equinoxes. However, because Earth's axial tilt does not affect the transmitted power, equinoctial geometry also provides an upper bound on the performance of an SSPS outside of eclipse.

Under these assumptions, the SSPS's true anomaly, ν, and the receiving station's angular position, θ, fully describe the positions of the SSPS and receiving station in Earth's equatorial plane. ν and θ respectively describe the angular positions of the SSPS and receiving station relative to $\hat{X}$ and are given by

$$\nu = n\,(t - t_0) + \nu_0 \tag{4}$$

7

$$\theta = \omega_{\oplus} (t - t_0) + \theta_0 \tag{5}$$

where n is the orbit's mean motion and $\omega_{\oplus}$ is the rotation rate of Earth about its axis. Note that for eccentric orbits, an expression analogous to Eq. (4) can be written by replacing the true anomaly with the mean anomaly [22]. In this paper, the SSPS and receiving station are assumed to start at local noon, i.e., at $\theta_0 = \nu_0 = 0°$, to facilitate comparisons between different orbit altitudes.

The angular position of a spacecraft relative to a point on Earth is typically described by its azimuth and elevation angles where the elevation angles above the horizon are restricted to the interval $[0°, 90°]$ [23]. However, for the two-dimensional scenario depicted in Fig. 3, the need for an azimuth angle is eliminated by redefining the elevation angle in the interval $[0°, 180°]$ using

$$\delta' = \begin{cases} \pi - \delta & \text{if } \nu - \theta > 0 \\ \\ \delta & \text{otherwise} \end{cases} \tag{6}$$

where δ is given by Eq. (3) and ν, $\theta \in [0°, 360°)$. Assuming that the SSPS can transmit to the receiving station for elevation angles that exceed $5°$ above the horizon, then $\delta' \in [5°, 175°]$.

For an SSPS in a circular, equatorial orbit transmitting to an equatorial receiving station, the sun angle, squint angle, receiving station angular position, and elevation angle depicted in Fig. 3 fully characterize the problem geometry. These four angles are geometrically related by

$$\beta + \phi = \delta' + \theta - \frac{\pi}{2} \tag{7}$$

Equation (7) replaces Eqs. (1) and (2) for equatorial orbits and receiving stations. To simplify our notation, we define $\gamma = \delta' + \theta - \pi/2$, from which it follows that

$$\beta + \phi = \gamma \tag{8}$$

γ accounts for the position of the SSPS relative to the receiving station and captures all of the orbit-dependencies in the problem geometry. Note that for a spacecraft in GEO located at the same longitude as its equatorial ground station, $\delta' = \pi/2$ so $\gamma = \theta$.

C. Pointing Constraints

The set of sun and squint angles where each architecture can simultaneously see both the Sun and receiving station are now characterized. These sets are ultimately used to rank each architecture's relative performance in Sec. III.

The chosen SSPS architecture imposes limits on the maximum allowable sun and squint angles. For any planar PV surface, power is collected for all sun angles so long as the surface is not parallel to or facing away from the Sun. Similarly, for any planar RF surface, power is transmitted for all squint angles so long as the surface is not parallel to or facing away from the receiving station. For a single-sided PV or single-sided RF module, these pointing constraints are

8
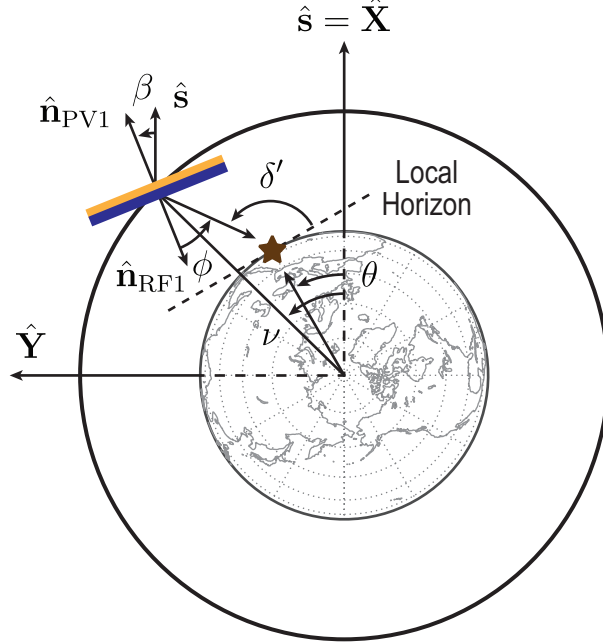
Fig. 3   Relative geometry between the SSPS, Sun, and receiving station for an SSPS in a circular, equatorial orbit transmitting to an equatorial receiving station. Even though the figure depicts the PV1RF1 SSPS, this geometry is equally applicable for any architecture.

expressed by the following domains for β:

$$\mathcal{D}_{\text{PV1}} = \left\{ \beta : -\frac{\pi}{2} < \beta < \frac{\pi}{2} \right\} \tag{9}$$

$$\mathcal{D}_{\text{RF1}} = \left\{ \beta : -\frac{\pi}{2} < \phi < \frac{\pi}{2} \right\} \tag{10}$$

where β is related to ϕ through Eqs. (1) and (2). Equations (9) and (10) are geometric requirements for planar surfaces to be oriented towards the Sun and receiving station, respectively. In any realistic SSPS, PV cell and antenna requirements may further restrict the allowable sun and squint angles. However, for the discussion of SSPS mission geometry to remain completely general, these reduced sun and squint angle ranges are instead accounted for through the transmitted power function introduced in the next section.

For a dual-sided PV module, power is collected for all sun angles so long as the surface is not oriented parallel to the Sun. Likewise, for a dual-sided RF module, power is transmitted for all squint angles so long as the surface is not oriented parallel to the receiving station. Hence, the following limits on β and ϕ apply for dual-sided modules:

$$\mathcal{D}_{\text{PV2}} = \left\{ \beta : -\pi \leq \beta < \pi \text{ and } \beta \neq \pm\frac{\pi}{2} \right\} \tag{11}$$

$$\mathcal{D}_{\text{RF2}} = \left\{ \beta : -\pi \leq \phi < \pi \text{ and } \phi \neq \pm\frac{\pi}{2} \right\} \tag{12}$$

9

If $\beta = \pm\pi/2$ or $\phi = \pm\pi/2$, zero power is transmitted, meaning we can account for these constraints implicitly through the transmitted power function instead of explicitly through $\mathcal{D}_{\text{PV2}}$ and $\mathcal{D}_{\text{RF2}}$. Hence, the following forms of Eqs. (11) and (12) are equivalent:

$$\mathcal{D}_{\text{PV2}} = \left\{ \beta : -\pi \leq \beta < \pi \right\} \tag{13}$$

$$\mathcal{D}_{\text{RF2}} = \left\{ \beta : -\pi \leq \phi < \pi \right\} \tag{14}$$

For power transmission, the admissible domain for β is the intersection of the domains corresponding to the applicable PV and RF surface pointing constraints, e.g. $\mathcal{D}_{\text{PV1}} \cap \mathcal{D}_{\text{RF2}}$ is the admissible domain for a PV1RF2 SSPS. The following relationships between the domains for the four SSPS architectures hold:

$$(\mathcal{D}_{\text{PV1}} \cap \mathcal{D}_{\text{RF1}}) \subset \left\{ \begin{array}{c} (\mathcal{D}_{\text{PV2}} \cap \mathcal{D}_{\text{RF1}}) = \mathcal{D}_{\text{RF1}} \\[2mm] (\mathcal{D}_{\text{PV1}} \cap \mathcal{D}_{\text{RF2}}) = \mathcal{D}_{\text{PV1}} \end{array} \right\} \subset (\mathcal{D}_{\text{PV2}} \cap \mathcal{D}_{\text{RF2}}) \tag{15}$$

from which it follows that any sun angle typically satisfies either the PV2RF1 or PV1RF2 pointing constraints, but not necessarily both.

Several simplifications can be made using the assumptions of the restricted power-optimal guidance problem. The single and dual-sided PV domains, Eqs. (9) and (13), are unchanged. However, Eq. (8) can be used to rewrite the single and dual-sided RF domains as

$$\mathcal{D}_{\text{RF1}} = \left\{ \beta : \gamma - \frac{\pi}{2} < \beta < \gamma + \frac{\pi}{2} \right\} \tag{16}$$

$$\mathcal{D}_{\text{RF2}} = \left\{ \beta : \gamma - \pi < \beta \leq \gamma + \pi \right\} \tag{17}$$

The resulting domains describing the pointing constraints for the equatorial case are summarized in Table 1. Note that in Table 1, $\mathcal{D}_{\text{PV2}} \cap \mathcal{D}_{\text{RF2}} = \mathcal{D}_{\text{PV2}} = \mathcal{D}_{\text{RF2}}$ because both $\mathcal{D}_{\text{PV2}}$ and $\mathcal{D}_{\text{RF2}}$ encompass the entire range of β.

Table 1   Domains corresponding to sun and squint angle limits for the four planar SSPS architectures under the assumptions of the restricted power-optimal guidance problem.

Architecture	Domain
PV1RF1	$\mathcal{D}_{\text{PV1}} \cap \mathcal{D}_{\text{RF1}}$
PV2RF1	$\mathcal{D}_{\text{PV2}} \cap \mathcal{D}_{\text{RF1}} = \mathcal{D}_{\text{RF1}}$
PV1RF2	$\mathcal{D}_{\text{PV1}} \cap \mathcal{D}_{\text{RF2}} = \mathcal{D}_{\text{PV1}}$
PV2RF2	$\mathcal{D}_{\text{PV2}} \cap \mathcal{D}_{\text{RF2}} = \mathcal{D}_{\text{PV2}} = \mathcal{D}_{\text{RF2}}$

Under the assumptions of the restricted power-optimal guidance problem, the domains corresponding to the pointing constraints are parameterized by a single variable, γ, which describes the position of the SSPS relative to the receiving station. To illustrate the consequences of Eq. (15), Fig. 4 depicts these domains for PV1RF1, PV2RF1, and PV1RF2

SSPSs for various values of γ. The PV2RF2 case is excluded from Fig. 4 because its domain encompasses the entire range of β. Figure 4 only considers values of γ corresponding to the left-half orbit plane because the problem geometry is symmetric about the sun vector.
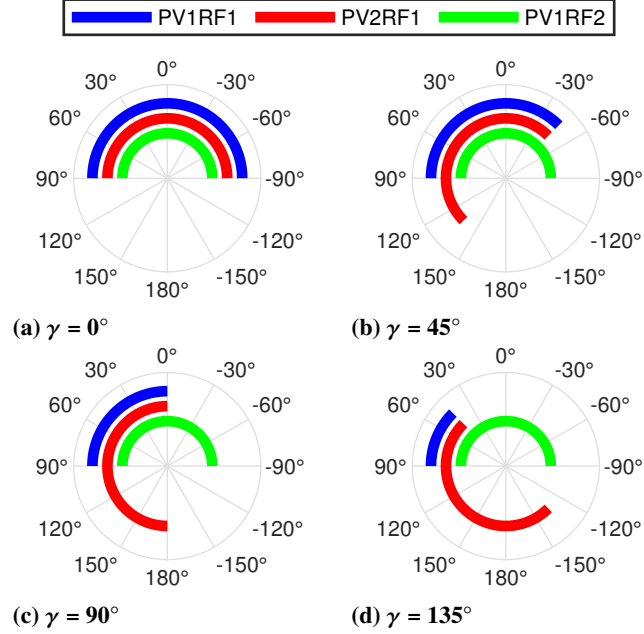
Fig. 4 Sun angle domains corresponding to the pointing constraints for PV1RF1, PV2RF1, and PV1RF2 SSPSs under the assumptions of the restricted power-optimal guidance problem. The polar angle is the sun angle, β. The outer, middle, and inner arcs denote PV1RF1, PV2RF1, and PV1RF2, respectively.

The domains corresponding to the PV2RF1 and PV1RF2 pointing constraints span a semicircle. $\mathcal{D}_{\text{PV1}}$ is independent of γ because it is defined about the inertially-fixed sun vector. Conversely, $\mathcal{D}_{\text{RF1}}$ is dependent on γ because it is defined about the orbit-varying slant vector. Hence, the PV2RF1 domain rotates as γ varies throughout the orbit but the PV1RF2 domain always remains fixed. The PV1RF1 domain is the intersection of the PV2RF1 and PV1RF2 domains. As a result, as γ increases, the PV1RF1 domain rotates and its range decreases. These phenomena are depicted in Fig. 4 and have important performance implications that are discussed in Sec. III.

D. Transmitted Power and Geometric Efficiency

The total power density per unit aperture area transmitted by an SSPS is expressed as the following product:

$$W_t(\beta, \phi) = \mathbb{1}(\mathbf{r})\, W_{\text{SF}}\, \eta_{\text{PV}}\, \eta_{\text{DC-RF}}\, \eta_{\text{Tx}}\, \text{PV}(\beta)\, \text{RF}(\phi)\, \text{AF}(\phi) \tag{18}$$

where

W_{SF} = 1,361 W/m^2 is the incident solar flux

η_{PV} is the optical-to-electrical power conversion efficiency of the PV cells

$\eta_{\text{DC-RF}}$ is the DC-to-RF conversion efficiency of the system

η_{Tx} is the antenna transmit efficiency due to impedance mismatching between the RF source and antenna

$\text{PV}(\beta)$ is the efficiency of the PV cells as a function of the sun angle

$\text{RF}(\phi)$ is the efficiency of a single antenna in the phased array as a function of the squint angle

$\text{AF}(\phi)$ is the phased array factor

The phased array factor modifies the single antenna efficiency to account for the influence of multiple emitters in a phased array [24]. Beam-steering of the phased array is captured by the squint angle dependencies of the antenna efficiency and phased array factor. $\mathbb{1}(\mathbf{r})$ is an orbit-dependent indicator function defined by

$$\mathbb{1}(\mathbf{r}) = \begin{cases} 1 & \text{if not in eclipse and above the horizon} \\ 0 & \text{otherwise} \end{cases} \tag{19}$$

Including $\mathbb{1}(\mathbf{r})$ in the definition of W_t guarantees that $W_t = 0$ when the SSPS is either in eclipse or below the horizon. Note that Eq. (18) assumes that $\text{PV}(\beta)$, $\text{RF}(\phi)$, and $\text{AF}(\phi)$ have no radial (azimuthal) dependencies.

$\text{PV}(\beta)$, $\text{RF}(\phi)$, and $\text{AF}(\phi)$ must satisfy several properties to accurately model the transmitted power. To guarantee $W_t \geq 0 \ \forall \ \beta, \phi$, $\text{PV}(\beta)$, $\text{RF}(\phi)$, and $\text{AF}(\phi)$ must all be positive semidefinite. Likewise, for the most general (PV2RF2) case, the SSPS's attitude is modulo $180°$, from which it follows that W_t must be π-periodic. Because the product of π-periodic functions is also π-periodic, the π-periodicity of W_t is guaranteed by requiring that $\text{PV}(\beta)$, $\text{RF}(\phi)$, and $\text{AF}(\phi)$ are all π-periodic. To account for the other three SSPS architectures, the domain of W_t is restricted using the appropriate sun and squint angle limits from Sec. II.C instead of redefining W_t for each architecture.

$\text{PV}(\beta)$, $\text{RF}(\phi)$, and $\text{AF}(\phi)$ are required to be even functions of their respective arguments. Symmetric functions are necessary for the transmitted power density to be radially independent. Finally, $\text{PV}(\beta)$ must account for the reduction in the effective solar collecting area as the magnitude of β increases. Similarly, the product $\text{RF}(\phi)\,\text{AF}(\phi)$ must account for the reduction in the effective transmit aperture area as ϕ increases. As a result, it is assumed that $\text{PV}(\beta)$, $\text{RF}(\phi)$, and $\text{AF}(\phi)$ are unimodal functions of their respective arguments in each interval of π centered at $i\pi \ \forall \ i \in \mathbb{Z}$. A unimodal function has only a single unique maximum (or minimum) in a given interval. Even though specific forms for $\text{PV}(\beta)$, $\text{RF}(\phi)$, and $\text{AF}(\phi)$ are used for the subsequent examples, the results and trends presented in this paper hold irrespective of their particular forms so long as the above assumptions are satisfied.

The examples in this paper assume planar (non-concentrated) PV surfaces with minimum acceptance angles of $5°$. The efficiency of a planar PV surface is approximated by a cosine loss, i.e., for local sun angles that exceed the minimum acceptance angle, $\text{PV}(\beta) = |\cos(\beta)|$. Figure 5 then plots the variation of the antenna efficiency with ϕ. This variation has been obtained from electromagnetic simulations of the near-isotropic patch antennas forming the RF layer described in [10]. Lastly, the phased array factor is approximated by a cosine loss, i.e., $\text{AF}(\phi) = |\cos(\phi)|$.
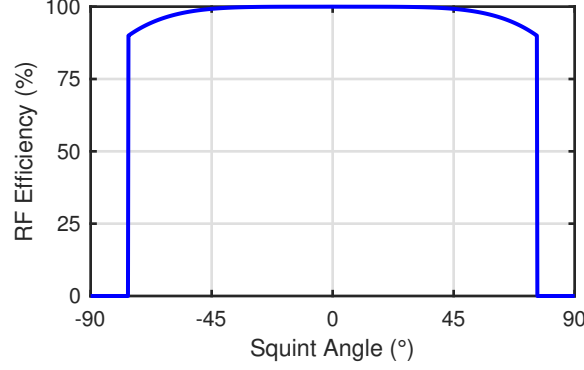
Fig. 5 **Variation of antenna efficiency with squint angle for the near-isotropic patch antennas described in [10]. The maximum allowable squint angle is 76°. The antenna efficiency is a periodic, symmetric function with a fundamental period of 180°.**

Within the scope of this paper, W_{SF}, η_{PV}, $\eta_{\text{DC-RF}}$, and η_{Tx} are constants. As a result, a normalized transmitted power density can be defined that only depends on the problem geometry in Fig. 2, as follows:

$$G(\beta, \phi) = \frac{W_t(\beta, \phi)}{W_{\text{SF}}\, \eta_{\text{PV}}\, \eta_{\text{DC-RF}}\, \eta_{\text{Tx}}} = \mathbb{1}(\mathbf{r})\, \text{PV}(\beta)\, \text{RF}(\phi)\, \text{AF}(\phi) \tag{20}$$

G is referred to as the geometric efficiency because it includes all of the geometric dependencies in the transmitted power density. Since G is simply a scaling of W_t, maximizing the geometric efficiency maximizes the transmitted power and vice versa. Likewise, since W_t is π-periodic, G is also π-periodic.

For the restricted power-optimal guidance problem, substituting Eq. (8) into Eq. (20) and replacing $\mathbf{r}$ with ν allows Eq. (20) to be rewritten as

$$G(\beta) = \mathbb{1}(\nu)\, \text{PV}(\beta)\, \text{RF}(\gamma - \beta)\, \text{AF}(\gamma - \beta) \tag{21}$$

Under these assumptions, G is a scalar function of β for a given γ. Equation (21) explicitly shows that the orientation that maximizes the transmitted power only depends on the relative SSPS-Sun-receiving station geometry and that this orientation is not necessarily the same as the orientation that maximizes the solar power collected.

E. Power-Optimal Guidance Problem

The power-optimal guidance problem determines the attitude trajectory that maximizes the total power transmitted to a receiving station. It is defined as follows:

Problem 1 (Continuous Power-Optimal Guidance Problem):

$$\underset{\beta(t), \phi(t)}{\text{maximize}} \quad E_t(\beta(t), \phi(t)) \tag{22}$$

subject to Eqs. (1), (2), and $\beta(t) \in \mathcal{D}_{\text{PV}} \cap \mathcal{D}_{\text{RF}}$. $\mathcal{D}_{\text{PV}}$ and $\mathcal{D}_{\text{RF}}$ are the domains corresponding to the applicable sun and

13

squint angle limits from Sec. II.C and

$$E_t = \int_{t_0}^{t_f} W_t(\beta(t), \phi(t)) \, dt \tag{23}$$

is the total energy transmitted per unit aperture area. Problem 1 reduces to the restricted power-optimal guidance problem when the SSPS is in a circular, equatorial orbit transmitting to an equatorial receiving station, allowing Eqs. (1) and (2) to be replaced by Eq. (8).

Using Eqs. (18) and (20), Eq. (23) can be equivalently written as

$$E_t = \frac{W_{\text{SF}} \eta_{\text{PV}} \eta_{\text{DC-RF}} \eta_{\text{Tx}}}{n} \int_{\nu_0}^{\nu_f} G(\beta(\nu), \phi(\nu)) \, d\nu \tag{24}$$

for a circular orbit. The optimization approach involves discretizing the objective function. After discretizing $\nu \in [\nu_0, \nu_f)$ into N steps, the result is

$$\int_{\nu_0}^{\nu_f} G(\beta(\nu), \phi(\nu)) \, d\nu \approx \sum_{k=0}^{N-1} G(\beta_k, \phi_k) \left(\frac{\nu_f - \nu_0}{N-1} \right) \tag{25}$$

Eqs. (24) and (25) can then be used to write the discrete form of the power-optimal guidance problem as

Problem 2 (Discrete Power-Optimal Guidance Problem):

$$\underset{\beta_k, \phi_k, \ \forall \ k=0,\ldots,N-1}{\text{maximize}} \quad \sum_{k=0}^{N-1} G(\beta_k, \phi_k) \tag{26}$$

subject to Eqs. (1), (2), and $\beta_k \in \mathcal{D}_{\text{PV}} \cap \mathcal{D}_{\text{RF}}$. Problem 2 applies to an SSPS in an arbitrary circular orbit transmitting to an arbitrarily located receiving station. Equations (24)–(26) show that maximizing the instantaneous geometric efficiency at each true anomaly, i.e., at each time step, is equivalent to maximizing the total transmitted energy. For each $\nu_k \in [\nu_0, \nu_f)$, the Extreme Value Theorem [25] guarantees the existence of at least one optimal solution to Problem 2.

Finally, for the case of an SSPS in a circular, equatorial orbit transmitting to an equatorial receiving station, Eqs. (8) and (21) can be used to rewrite the power-optimal guidance problem as

Problem 3 (Discrete, Restricted Power-Optimal Guidance Problem):

$$\underset{\beta_k \ \forall \ k=0,\ldots,N-1}{\text{maximize}} \quad \sum_{k=0}^{N-1} G(\beta_k) \tag{27}$$

subject to $\beta_k \in \mathcal{D}_{\text{PV}} \cap \mathcal{D}_{\text{RF}}$. The optimal value of Problem 3's objective function is denoted

$$J_{\text{PV,RF}}^* = \sum_{k=0}^{N-1} G(\beta_k^*) \tag{28}$$

14

where $\beta_k^* \in \mathcal{D}_{\mathrm{PV}} \cap \mathcal{D}_{\mathrm{RF}}$ maximizes $G(\beta)$ at time step k. Any subsequent references in this paper to the power-optimal guidance problem refer to Problem 3.

III. Power-Optimality Theorem

In this section, geometric arguments are used to derive an inequality that relates the power transmitted by each of the four SSPS architectures under the assumptions of the restricted power-optimal guidance problem.

Theorem 1 (power-optimality): For $J_{\mathrm{PV1,RF1}}^*$, $J_{\mathrm{PV2,RF1}}^*$, $J_{\mathrm{PV1,RF2}}^*$, and $J_{\mathrm{PV2,RF2}}^*$ defined by Eq. (28),

$$J_{\mathrm{PV1,RF1}}^* \leq J_{\mathrm{PV2,RF1}}^* = J_{\mathrm{PV1,RF2}}^* = J_{\mathrm{PV2,RF2}}^* \tag{29}$$

Proof: The proof follows directly from the π-periodicity of the geometric efficiency function. The ranges of the domains for each of the four SSPS architectures are

$$\mathrm{range}\,(\mathcal{D}_{\mathrm{PV1}} \cap \mathcal{D}_{\mathrm{RF1}}) = |\pi - \mathrm{mod}(\gamma, 2\pi)| \leq \pi \tag{30}$$

$$\mathrm{range}\,(\mathcal{D}_{\mathrm{PV2}} \cap \mathcal{D}_{\mathrm{RF1}}) = \mathrm{range}\,(\mathcal{D}_{\mathrm{PV1}} \cap \mathcal{D}_{\mathrm{RF2}}) = \pi \tag{31}$$

$$\mathrm{range}\,(\mathcal{D}_{\mathrm{PV2}} \cap \mathcal{D}_{\mathrm{RF2}}) = 2\pi \tag{32}$$

where $\mathrm{mod}(a, b)$ denotes the remainder after division of a by b for $a, b \in \mathbb{R}$. The Extreme Value Theorem guarantees the existence of a global maximum in each interval of the fundamental period of a periodic function. Since the geometric efficiency function is π-periodic and the ranges of the solution domains for PV2RF1, PV1RF2, and PV2RF2 are all equal to multiples of the fundamental period, it follows that

$$J_{\mathrm{PV2,RF1}}^* = J_{\mathrm{PV1,RF2}}^* = J_{\mathrm{PV2,RF2}}^* \tag{33}$$

However, because the range of the PV1RF1 solution domain is always less than or equal to the fundamental period of 180°, there is no guarantee that the PV1RF solution domain encompasses a global maximizer of the geometric efficiency. As a result,

$$J_{\mathrm{PV1,RF1}}^* \leq J_{\mathrm{PV2,RF1}}^* = J_{\mathrm{PV1,RF2}}^* = J_{\mathrm{PV2,RF2}}^* \tag{34}$$

which completes the proof.

The following strong form of the theorem holds:

Theorem 2 (strong power-optimality): For $J_{\mathrm{PV1,RF1}}^*$, $J_{\mathrm{PV2,RF1}}^*$, $J_{\mathrm{PV1,RF2}}^*$, and $J_{\mathrm{PV2,RF2}}^*$ defined by Eq. (28),

$$J_{\mathrm{PV1,RF1}}^* < J_{\mathrm{PV2,RF1}}^* = J_{\mathrm{PV1,RF2}}^* = J_{\mathrm{PV2,RF2}}^* \tag{35}$$

Proof: The strict inequality in Eq. (35) is a consequence of the fact that for a single-sided SSPS, there exist values of γ for which either $G(\beta) = 0$, $\mathcal{D}_{\text{PV1}} \cap \mathcal{D}_{\text{RF1}} = \emptyset$, or both for all $\beta \in \mathcal{D}_{\text{PV1}} \cap \mathcal{D}_{\text{RF1}}$.

An example of this is shown in Fig. 6 which depicts the PV1RF1 SSPS when both the spacecraft and receiving station are at local midnight. Figure 6 shows that the PV1RF1 SSPS cannot simultaneously point both its PV surface towards the Sun and its RF surface towards the receiving station in the vicinity of local midnight. As a result, $G(\beta) = 0$ for all $\beta \in \mathcal{D}_{\text{PV1}} \cap \mathcal{D}_{\text{RF1}}$ in the vicinity of local midnight. This decreases the performance of the PV1RF1 SSPS relative to the three dual-sided SSPSs.

(a) PV surface oriented towards Sun (b) RF surface oriented towards receiving station
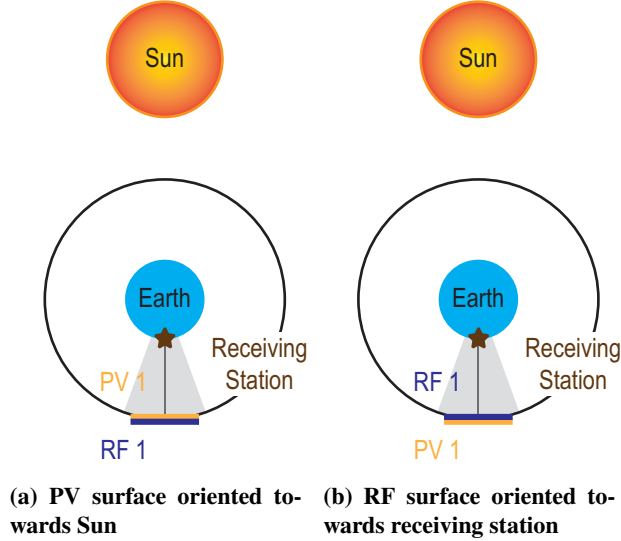
Fig. 6   At local midnight, either the PV surface or the RF surface of the PV1RF1 SSPS can be oriented towards the Sun and receiving station, not both. The SSPS cannot transmit in the shaded region of the orbit.

There are two important corollaries of the power-optimality theorem:

1) The performance of the PV1RF1 SSPS is at best equal to the performance of a dual-sided SSPS. In other words, the PV1RF1 SSPS provides a lower bound for the power transmitted by a dual-sided SSPS because a dual-sided SSPS can always operate as a PV1RF1 SSPS. For the solutions to the restricted power-optimal guidance problem considered in this paper, the performance of the PV1RF1 SSPS is always worse than the performance of the dual-sided SSPSs.

2) The total powers transmitted by PV2RF1, PV1RF2, and PV2RF2 SSPSs are equivalent, i.e., the total power transmitted by a PV2RF2 SSPS does not increase relative to either PV2RF1 or PV1RF2 SSPSs. However, there is typically a substantial performance benefit (potentially up to 50%) realized by having either two PV surfaces or two RF surfaces, as shown in Secs. IV and V.

The theorem is a direct result of the pointing constraints, meaning it is independent of the orientation(s) that maximize the transmitted power. As a result, even though all three dual-sided SSPSs transmit equivalent powers, their corresponding optimal attitude trajectories are not necessarily identical. A decision to use a specific dual-sided architecture for a

specific mission must therefore be driven by additional factors, such as cost or manufacturability. Moreover, because the pointing constraints for the restricted power-optimal guidance problem are independent of the orbit's altitude and eccentricity, the theorem is also independent of altitude and eccentricity.

IV. Solutions to the Restricted Power-Optimal Guidance Problem

This section solves the restricted power-optimal guidance problem for SSPSs in the three circular, equatorial orbits listed in Table 2 transmitting to an equatorial receiving station. Solutions are sought that are periodic with respect to time so that system performance does not change on a daily basis. Hence, only orbits with periods that are integer multiples of a sidereal day are simulated. Considering solutions for geostationary Earth orbit (GEO), a medium Earth orbit (MEO), and a low Earth orbit (LEO) highlights differences between the solutions as the orbit altitude decreases. In particular, the MEO and LEO cases highlight the effects of finite duration receiving station passes and receiving station relative motion on the solutions.

Table 2   Orbit altitudes for solutions to the restricted power-optimal guidance problem

Label	Orbit Altitude (km)	Orbits/Sidereal Day
GEO	35,876	1
MEO	20,184	2
LEO	881	14

Most space solar power concepts in the literature consider spacecraft in GEO (e.g. [4]). However, there are potential advantages of placing an SSPS outside of GEO. For example, even though satellites in MEO experience a considerably harsher radiation environment compared to GEO [26], MEO can be advantageous because it is largely unoccupied (with several notable exceptions, e.g. GPS) and allows a small constellation of satellites to achieve persistent coverage of a single location on Earth. Moreover, launch costs per kilogram of payload to MEO and LEO are lower than to GEO.

A. Solution Approach

The restricted power-optimal guidance problem (Problem 3) is solved using direct transcription and local optimization. The orbit is first discretized into into N steps, after which local optimization is used to find the orientation that maximizes the geometric efficiency at each $v_k \in [v_0, v_f)$ for $k = 0, 1, \ldots, N-1$. For the optimization at each v_k, a meta-optimization routine that couples a grid search algorithm with a non-gradient based optimization algorithm (e.g. a golden section search [27]) is implemented. The grid search identifies intervals containing maximizer(s) of the geometric efficiency at each v_k, after which the optimizer solves for the value(s) of the maximizer(s) to a specified precision. A non-gradient based optimization algorithm is used because the geometric efficiency function is not required to have continuous first derivatives.

For each orbit in Table 2, Problem 3 is initially solved for a PV2RF2 SSPS. Results for the remaining three SSPS architectures are obtained by constraining the set of PV2RF2 solutions. Solutions for the PV2RF2 SSPS are referred to as solutions to the *unconstrained* (restricted power-optimal guidance) problem. Likewise, solutions for the other three architectures are referred to as *constrained* solutions.

B. Properties of the Geometric Efficiency Function

Some useful properties of the geometric efficiency function are first investigated to provide context for the restricted power-optimal guidance solutions. Specifically, the effects of changing γ on the maximizers of the geometric efficiency are investigated to highlight the multiplicity of these maximizers and a consequence of dual-sided operations. To this end, "snapshots" of the geometric efficiency are considered at various values of γ. γ is used to parameterize the orbit-dependencies in the problem geometry so that any conclusions are applicable to any equatorial orbit. Physical intuition for γ can be developed by recalling that $\gamma = \theta$ for GEO. Moreover, because the problem geometry is symmetric about the sun vector, only values of γ corresponding to the left-half orbit plane are considered. The results can then be extended to the right-half orbit plane by reflecting them about the sun vector.

Figure 7 plots the geometric efficiency as a function of the sun angle for a PV2RF2 SSPS at three different values of γ. The figure illustrates the π-periodicity of the geometric efficiency, namely that in any 360° interval of β, there are *at least* two maximizers of the geometric efficiency. This result shows that solutions to the power-optimal guidance problem for a PV2RF2 SSPS are not unique. One approach to circumventing this non-uniqueness is to use either the PV2RF1 or PV1RF2 solutions for the PV2RF2 solution because the PV2RF1 and PV1RF2 solutions are a subset of the non-unique PV2RF2 solutions, in accordance with Eq. (15). In this paper, unless otherwise stated, the PV2RF2 solution is represented by the PV2RF1 solution.

(a) $\gamma = 45°$ (b) $\gamma = 90°$ (c) $\gamma = 135°$
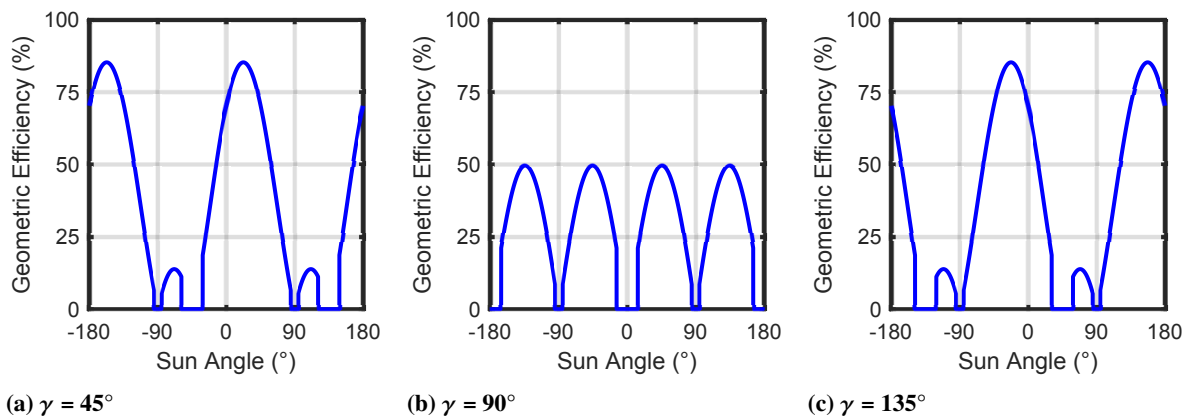
Fig. 7   Snapshots of the geometric efficiency for a PV2RF2 SSPS.

Next, the geometric efficiency's behavior in the vicinity of $\gamma = 90°$, as depicted in Fig. 7b, is considered. The figure shows that the geometric efficiency has four global maximizers, two each in each period of 180°. This has important

consequences for solutions to the power-optimal guidance problem.

To better understand these consequences, Figs. 8–10, overlay the PV2RF1, PV1RF2, and PV1RF1 constraints onto the geometric efficiency plots in Fig. 7. Figures 8a, 9a, and 10a show that for $\gamma = 45°$, only one global maximizer of the unconstrained problem simultaneously satisfies the constraints for all four SSPSs. This global maximizer corresponds to the solution for the PV1RF1 SSPS. Moreover, this observation holds throughout the first quarter of the orbit, i.e., for $\gamma \in [0°, 90°)$. Similarly, Figs. 8c and 9c show that for $\gamma = 135°$, each of the two unconstrained global maximizers satisfies either the PV2RF1 or PV1RF2 pointing constraints, not both. These global maximizers correspond to using either the second PV surface and the first RF surface or the first PV surface and the second RF surface for power collection and transmission, respectively. These observations hold throughout the second quarter of the orbit, i.e. for $\gamma \in (90°, 180°]$. In contrast, Fig. 10c shows that the pointing constraints force the PV1RF1 SSPS to operate at a significantly reduced geometric efficiency throughout the second quarter of the orbit.

(a) $\gamma = 45°$ (b) $\gamma = 90°$ (c) $\gamma = 135°$
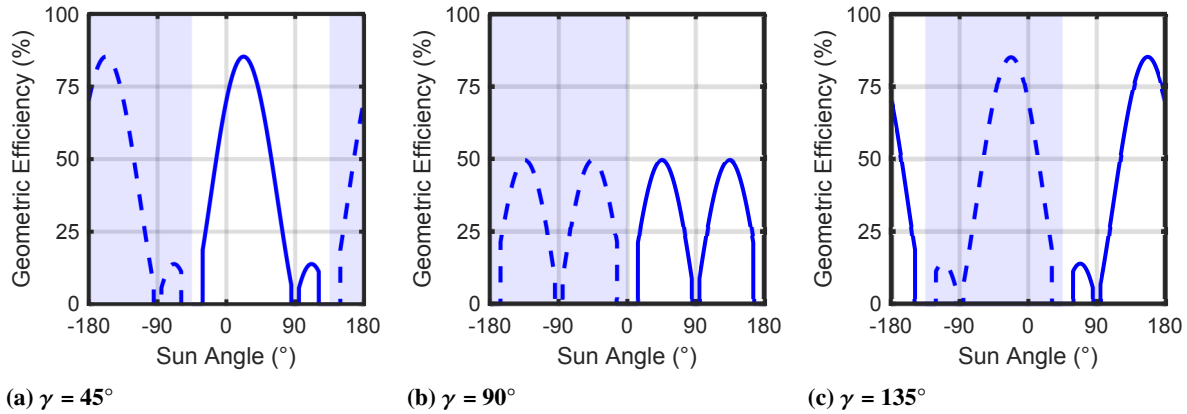
Fig. 8 Snapshots of the geometric efficiency for a PV2RF1 SSPS. Shaded regions violate the PV2RF1 pointing constraints.

(a) $\gamma = 45°$ (b) $\gamma = 90°$ (c) $\gamma = 135°$
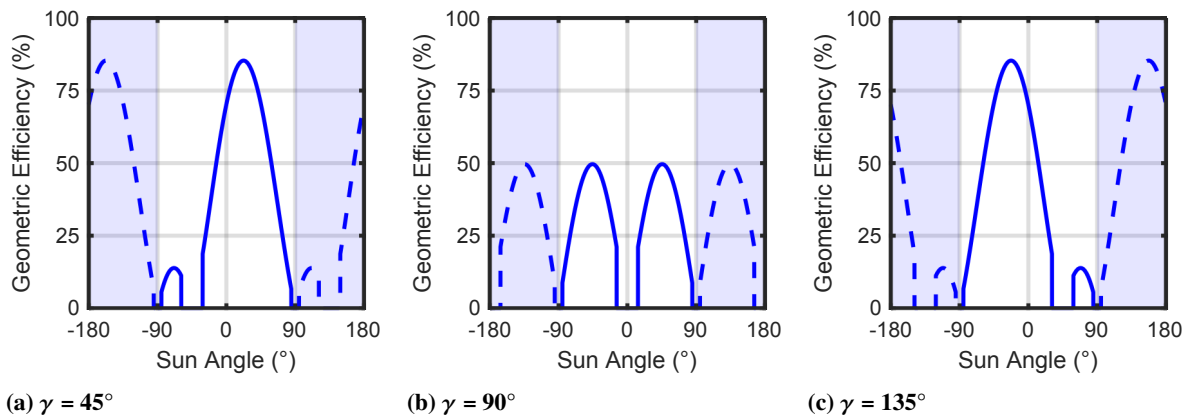
Fig. 9 Snapshots of the geometric efficiency for a PV1RF2 SSPS. Shaded regions violate the PV1RF2 pointing constraints.

(a) $\gamma = 45°$ (b) $\gamma = 90°$ (c) $\gamma = 135°$
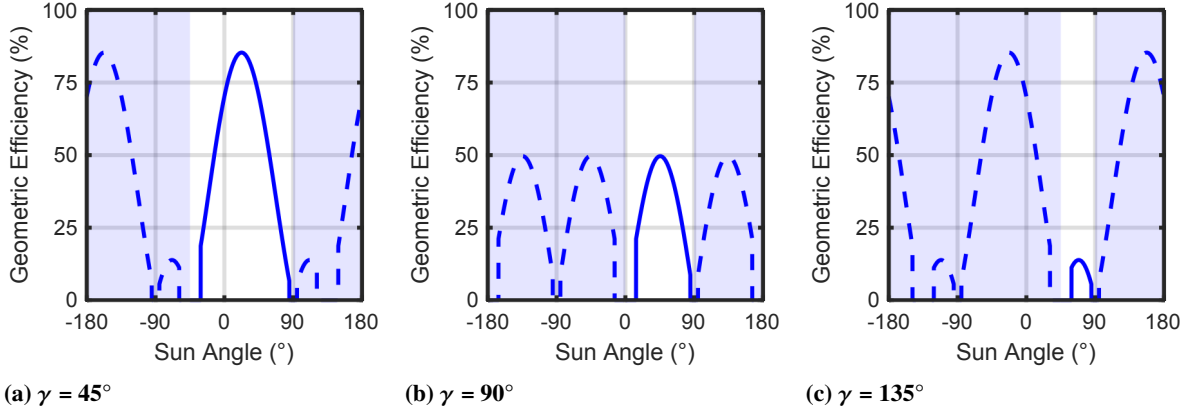
Fig. 10   Snapshots of the geometric efficiency for a PV1RF1 SSPS. Shaded regions violate the PV1RF1 pointing constraints.

Returning to Fig. 7b, there are four unconstrained global maximizers of the geometric efficiency when $\gamma = 90°$. Based on Figs. 8b and 9b, two unconstrained global maximizers each satisfy the PV2RF1 and PV1RF2 pointing constraints. However, only a single unconstrained global maximizer satisfies each of these constraints for $\gamma \in [0°, 90°)$ and $\gamma \in (90°, 180°]$. Since the unconstrained global maximizers for $\gamma \in [0°, 90°)$ and $\gamma \in (90°, 180°]$ occur in different quadrants of β, when $\gamma = 90°$, the solution must instantaneously "jump" from the maximizer in quadrant 1 to either the maximizer in quadrant 2 or 4, depending on whether a PV2RF1 or PV1RF2 SSPS is being considered. These jumps require instantaneous slews between two equally power-optimal orientations. Note that since an instantaneous slew requires an infinite acceleration, there is a singularity in the dynamics that realize a power-optimal attitude trajectory. Conversely, Fig. 10b shows that only a single unconstrained global maximizer satisfies the PV1RF1 constraints at $\gamma = 90°$. Due to these constraints, the optimum orientation for a PV1RF1 module varies continuously throughout the orbit so long as its geometric efficiency is non-zero.

Jumps are the cost of increased performance from dual-sided operations. They instantaneously reorient the spacecraft to decrease the local sun and squint angles on the active PV and RF surfaces, thereby increasing overall geometric efficiency. In practice, this means that jumps switch either the active PV or RF surface to best configure the SSPS for the relative geometry encountered in a particular region of its orbit.

For the geometry in Fig. 3, jumps occur when

$$\gamma = \pm(2i - 1)\frac{\pi}{2}, \qquad \forall\, i \in \mathbb{Z} \tag{36}$$

Equation (36) is a purely geometric condition that holds for any geometric efficiency function. Using Eq. (8) to rewrite

Eq. (36) results in:

$$\beta + \phi = \begin{cases} \pi/2 & \text{if } 0 \leq \gamma < \pi \\ 3\pi/2 & \text{if } \pi < \gamma < 2\pi \end{cases} \tag{37}$$

Thus, jumps occur when β and ϕ are complementary angles, i.e., when the vectors to the Sun and receiving station are orthogonal. Because Eqs. (36) and (37) only depend on γ, they are invariant to the orbit. However, since $\gamma = \delta' + \theta - \pi/2$ and δ' is a function of ν, the true anomaly corresponding to a jump is orbit-dependent. For a given orbit, substituting $\gamma = \delta' + \theta - \pi/2$ into Eq. (36) yields an equation that can be solved numerically for the true anomalies corresponding to each jump.

C. Geostationary Earth Orbit (GEO)

The restricted power-optimal guidance problem is next solved for a PV2RF2 SSPS in GEO. Solutions for the other three SSPS architectures are subsequently obtained by constraining the PV2RF2 solutions.

Figure 11 plots optimal orientation as a function of true anomaly for a PV2RF2 SSPS. Specifically, the local and global maximizers of the geometric efficiency function are plotted in Fig. 11a and the corresponding geometric efficiency profiles are plotted in Fig. 11b. Local and global maximizers/maxima are denoted by dashed and solid lines, respectively. Any path following a solid line in Fig. 11a is a non-unique globally optimal solution for a PV2RF2 SSPS. Due to eclipsing, the geometric efficiency briefly drops to zero near local midnight, regardless of the orientation of the SSPS. As a result, straight lines are used to connect the optimum attitude trajectories through eclipse. Note that figures in this section plot the local and global maximizers in the interval $-360° \leq \beta \leq 360°$ to avoid artificially introducing discontinuities in the solutions due to 360° wrapping.

As a consequence of Eq. (15), all possible solutions for the three other architectures are also contained in Fig. 11a. These solutions can be readily visualized by overlaying the appropriate constraint regions onto Fig. 11a, as is done in Figs. 12b, 12c, and 13a for PV2RF1, PV1RF2, and PV1RF1, respectively. Due to the non-uniqueness of the PV2RF2 solutions, the PV2RF1 solution is chosen as the PV2RF2 solution, as denoted by the blue line in Fig. 12a.

In accordance with the power-optimality theorem, all three dual-sided SSPSs share the optimal geometric efficiency profile depicted in Fig. 12d. All three dual-sided SSPSs always operate at global maximizers of the geometric efficiency.

Whereas all of the dual-sided solutions are qualitatively similar, the geometry fundamentally changes the solution for the PV1RF1 case. Figure 6 shows that in the vicinity of local midnight, the PV1RF1 SSPS can only orient either its PV surface towards the Sun or its RF surface towards the receiving station, not both. Due to the geometry in the vicinity of local midnight, the sun and squint angles continually increase until one of the following happens: 1) the pointing constraints are violated, 2) the incident sun angle on the PV surface drops below its minimum acceptance angle, or 3) the transmitted squint angle on the RF surface exceeds its maximum allowable angle. As the sun and squint angles increase,

(a) **Local and global maximizers of the geometric efficiency.**

(b) **Geometric efficiency profiles corresponding to local and global maximizers.**
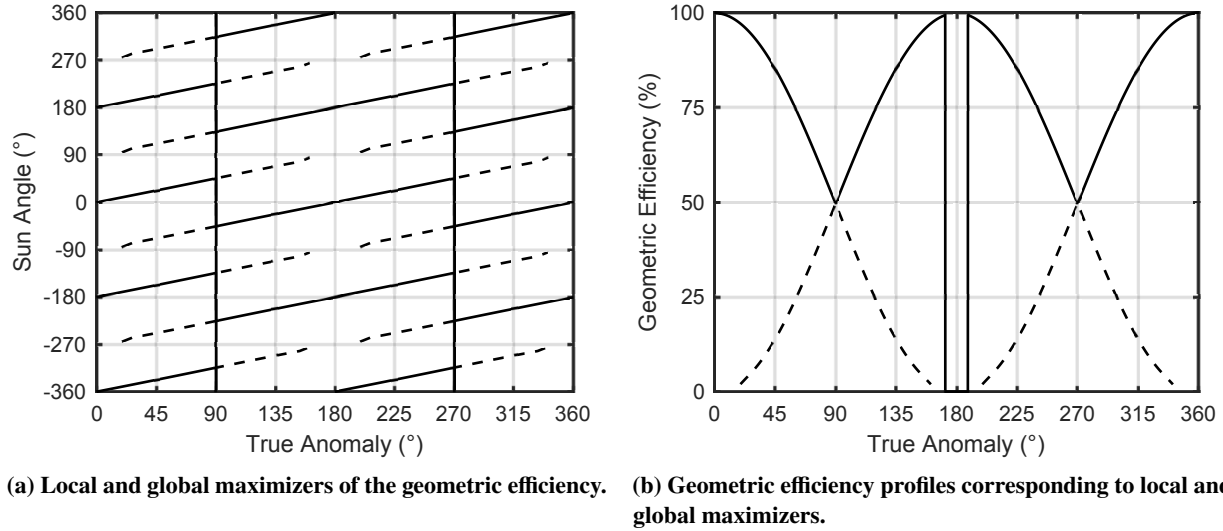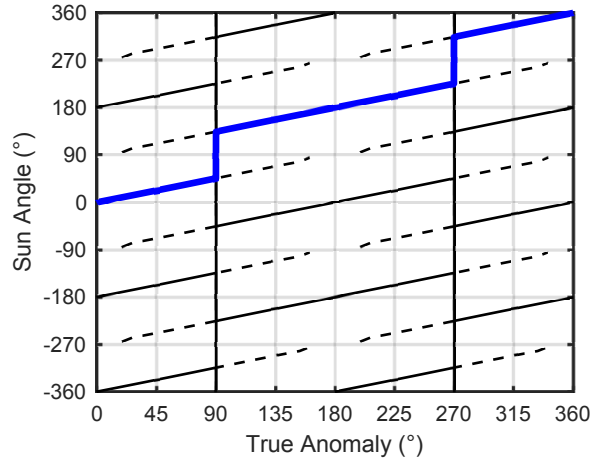
Fig. 11   Solutions to the restricted power-optimal guidance problem for a PV2RF2 SSPS in GEO. Solid and dashed lines respectively denote solutions corresponding to global and local maxima. Any path following a solid line is a globally optimal solution.

the geometric efficiency simultaneously decreases. For the system under consideration, the minimum PV acceptance angle is 5° (corresponding to a maximum locally incident sun angle of 85°) and the maximum transmitted squint angle is 76°. As a result, the PV1RF1 SSPS first reaches a point in the vicinity of local midnight where the maximum allowable squint angle is reached, at which point the optimal solution increases the sun angle while keeping the squint angle fixed, as depicted in Fig. 13a. Once the geometry is such that both the maximum allowable sun and squint angles are both exceeded, the geometric efficiency drops to zero, as depicted in Fig. 13b. This explains why the PV1RF1 solution in Fig. 13 traces a path through Fig. 11a that includes both local and global maximizers of the unconstrained problem.

When the geometric efficiency is zero, any arbitrary attitude can be used to represent the solution. For simplicity, straight lines are chosen in Fig. 13a and all subsequent figures to represent solutions when the geometric efficiency is zero. In Fig. 13a, the straight line represents a slow slew maneuver that transitions the spacecraft between the two regions of the orbit where the required optimal sun and squint angles do not exceed the maximum allowable sun and squint angles, as opposed to the jumps that characterize the dual-sided solutions.

Finally, the optimal orientations for all four SSPS architectures are illustrated pictorially in Fig. 14. Figure 14 highlights that all four architectures share the same optimal orientations for $v \in [0°, 90°)$ and $v \in (270°, 360°)$. Moreover, Fig. 14 demonstrates that the relative geometry between the SSPS, Sun, and receiving station is always identical for the dual-sided SSPSs; the SSPS architecture only determines the combination of active PV and RF surfaces at any given point in the orbit.

(a) Trajectory for a PV2RF2 SSPS.
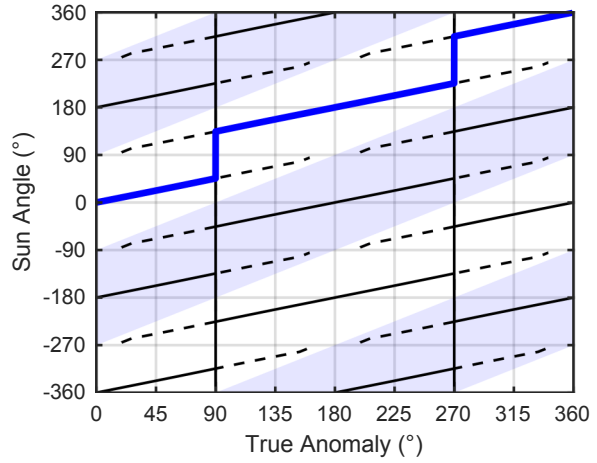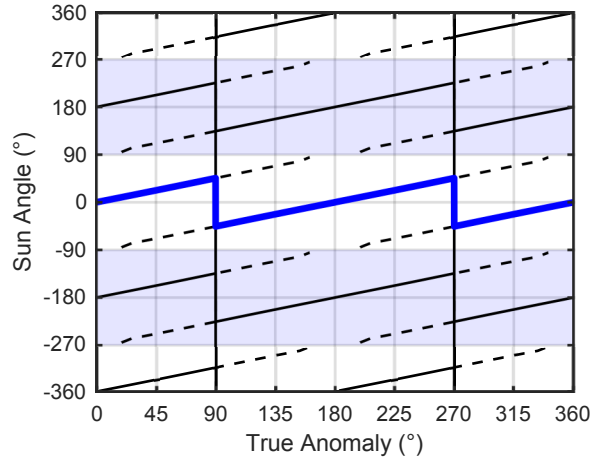
(b) Trajectory for a PV2RF1 SSPS.
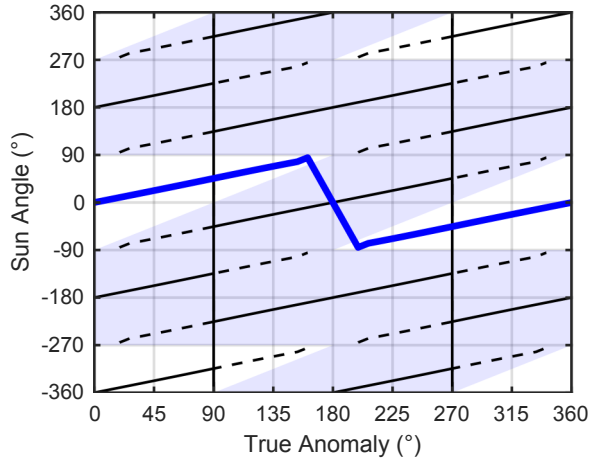

(c) Trajectory for a PV1RF2 SSPS.
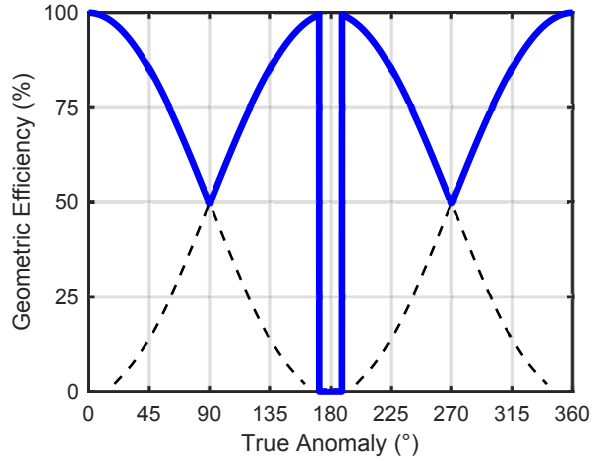
(d) Optimum geometric efficiency profile for dual-sided SSPSs.

Fig. 12   Solutions (blue) to the restricted power-optimal guidance problem for dual-sided SSPSs in GEO. All three dual-sided SSPSs share the same optimum geometric efficiency depicted in (d). Solid and dashed lines respectively denote solutions corresponding to global and local maxima of the unconstrained (PV2RF2) problem. Shaded regions violate pointing constraints.

D. Medium Earth Orbit (MEO)

Eclipsing and finite duration receiving station passes are responsible for the fundamental differences between power-optimal guidance for GEO and for any other orbit. Specifically, because the SSPS requires sunlight and must be above the horizon relative to the receiving station for power transmission, the power-optimal guidance solutions are undefined over regions of an orbit where neither condition is satisfied.

To illustrate this, the case of an SSPS in a 20,184 km altitude circular equatorial MEO transmitting to an equatorial receiving station is considered next. At this altitude, the SSPS completes two orbits per sidereal day. Assuming the SSPS and receiving station both start at $\nu_0 = \theta_0 = 0°$, then the SSPS is only in view of the receiving station at the

(a) Power-optimal attitude trajectory.
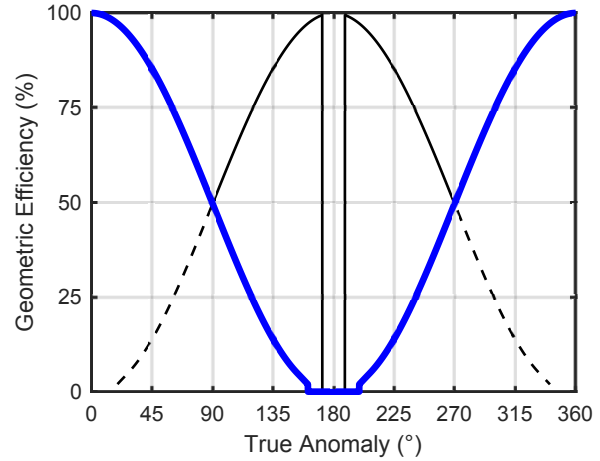
(b) Optimum geometric efficiency profile.

Fig. 13   Solution (blue) to the restricted power-optimal guidance problem for the PV1RF1 SSPS in GEO. Solid and dashed lines respectively denote solutions corresponding to global and local maxima of the unconstrained (PV2RF2) problem. Shaded regions violate pointing constraints. A straight line is used to connect discontinuous pieces of the solution.

| PV | RF-transparent PV | no transmission |
| RF | optically-transparent RF | |

(a) PV2RF2   (b) PV2RF1   (c) PV1RF2   (d) PV1RF1
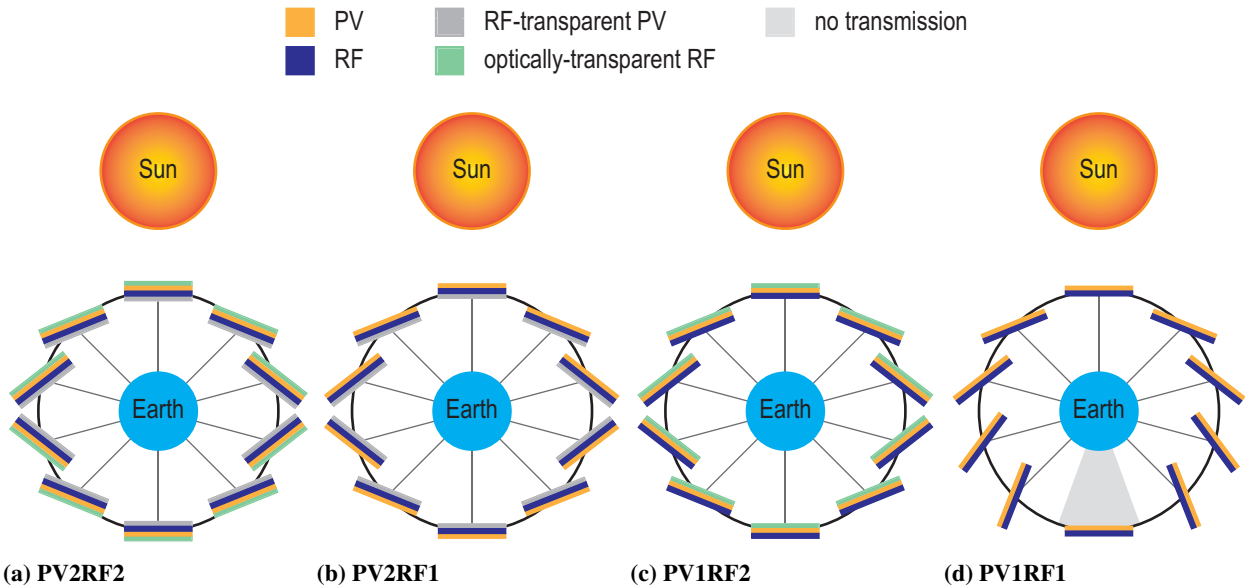
Fig. 14   Illustrations of the optimum orientations for single and dual-sided SSPSs in GEO. The geometric efficiency is zero in the shaded region in (d).

beginning of the first orbit and the end of the second orbit, as depicted by the elevation angle plot in Fig. 15. For an equatorial MEO, eclipse periods occur in the vicinity of $\nu = 180°$ and $\nu = 540°$. Hence, with $\nu_0 = \theta_0 = 0°$, the SSPS is never in view of the receiving station during eclipse. However, between passes, the SSPS is below the horizon relative to the receiving station. As a result, the geometric efficiency is zero between passes irrespective of the SSPS's orientation, which implies that any arbitrary attitude can be chosen to represent the solution between passes. For simplicity, straight

24

lines are again chosen for the solutions between passes.
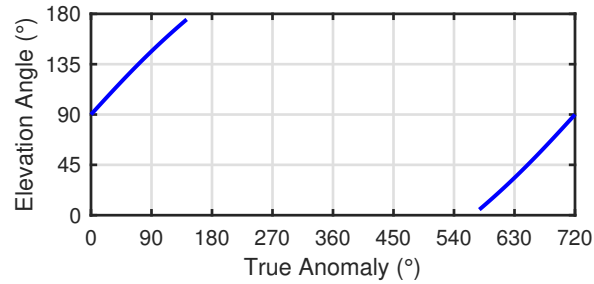
Fig. 15   Elevation angles for two orbits in MEO.

Figure 16 shows the restricted power-optimal guidance solutions for an SSPS in the circular, equatorial MEO transmitting to an equatorial receiving station. When the SSPS is in view of the receiving station, the solutions are qualitatively similar to the solutions for GEO. For example, the MEO and GEO solutions both feature jumps of the same magnitude that occur at different true anomalies, in accordance with Eq. (36). Note that the PV2RF1 solution is again used as the PV2RF2 solution because the unique solution for the PV2RF1 case is a subset of the non-unique solutions for the PV2RF2 case, in accordance with Eq. (15).

Figure 17 then plots the PV1RF1 solution for an SSPS in MEO. Again, this solution is qualitatively similar to its GEO counterpart, except that the slow slew maneuver occurs over a significantly wider range of true anomalies ($\approx 435°$) due to the long duration between passes.

Lastly, the optimum orientations for the four SSPSs throughout each orbit are depicted in Fig. 18. The shaded regions in Fig. 18 correspond to the areas of each orbit where the SSPS is not in view of the receiving station. As was observed in the GEO case, all four SSPSs again share the same optimal orientations for $\theta \in [0°, 90°)$ and $\theta \in (540°, 720)$ and all three dual-sided architectures again experience the same relative SSPS-Sun-receiving station geometry with the caveat that they may have different active PV and RF surfaces.

E. Low Earth Orbit (LEO)

Lastly, solutions to the restricted power-optimal guidance problem for an SSPS in an 881 km altitude LEO are presented. At this altitude, the SSPS completes 14 orbits per sidereal day. Due to the short duration of LEO receiving station passes (on the order of 10 minutes), the receiving station motion minimally affects the power-optimal guidance during each pass. However, the receiving station motion is critical for describing the reorientation maneuvers executed by the SSPS between passes. To emphasize some characteristics of the LEO solutions, solutions corresponding to passes over inertially-fixed receiving stations at $\theta = 0°, 45°, 90°,$ and $135°$ are first investigated for dual-sided and single-sided SSPSs in Figs. 19 and 20, respectively. Pictorial representations of these solutions are included in Fig. 21 where shading depicts the eclipse regions of each orbit. Note that the PV2RF1 solution is again used as the PV2RF2 solution, in
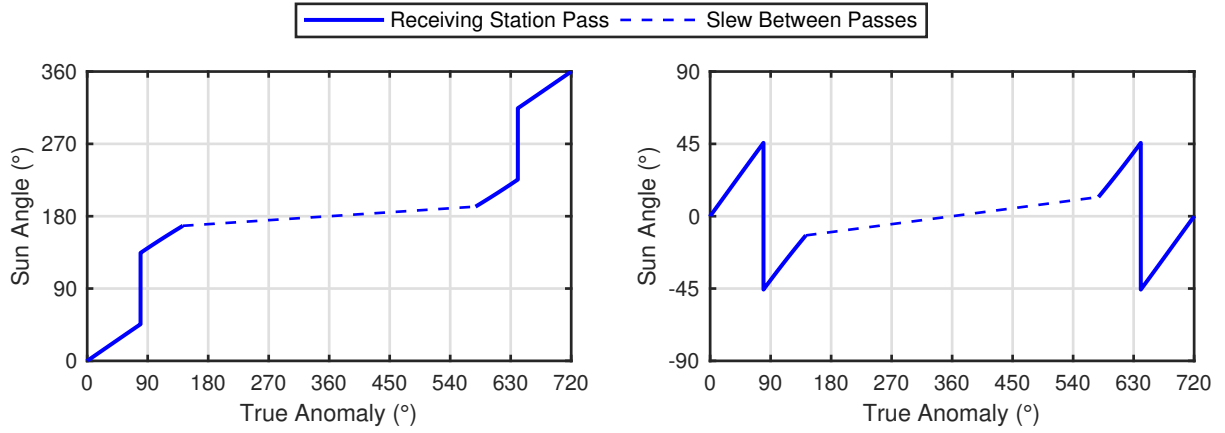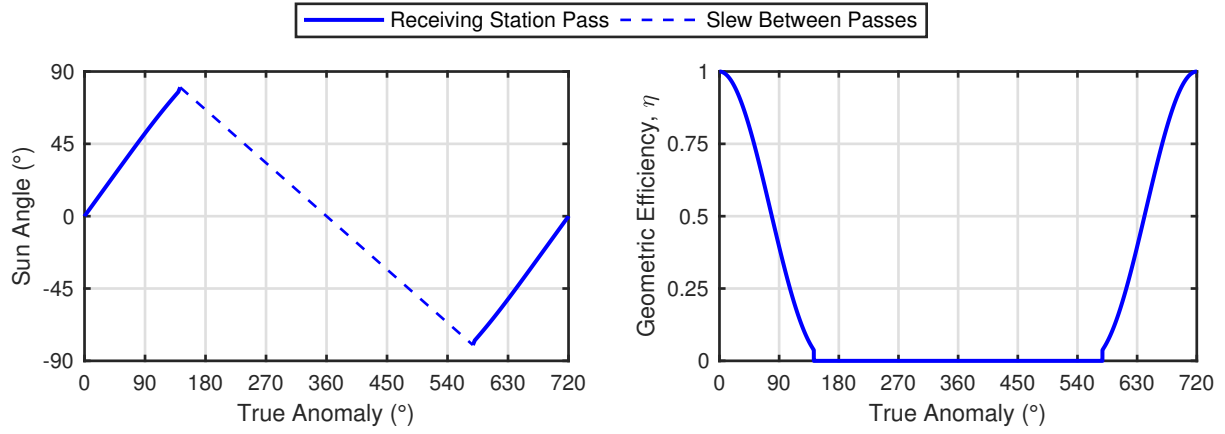
(a) Trajectory for PV2RF2 and PV2RF1 SSPSs.

(b) Trajectory for a PV1RF2 SSPS.
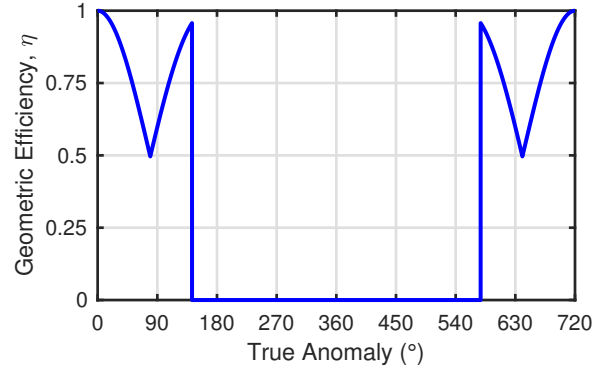
(c) Optimum geometric efficiency profile for dual-sided SSPSs.

Fig. 16 **Solutions to the restricted power-optimal guidance problem for dual-sided SSPSs for two orbits in MEO. All three dual-sided SSPSs share the same optimum geometric efficiency depicted in (c).**

(a) Power-optimal attitude trajectory.

(b) Optimum geometric efficiency profile.

Fig. 17 **Solution to the restricted power-optimal guidance problem for the PV1RF1 SSPS for two orbits in MEO.**

accordance with Eq. (15). The only caveat is that because the attitude of a PV2RF2 SSPS is modulo 180° and the attitude of a PV2RF1 SSPS is modulo 360°, the PV2RF2 solution may be offset by an integer multiple of 180° relative
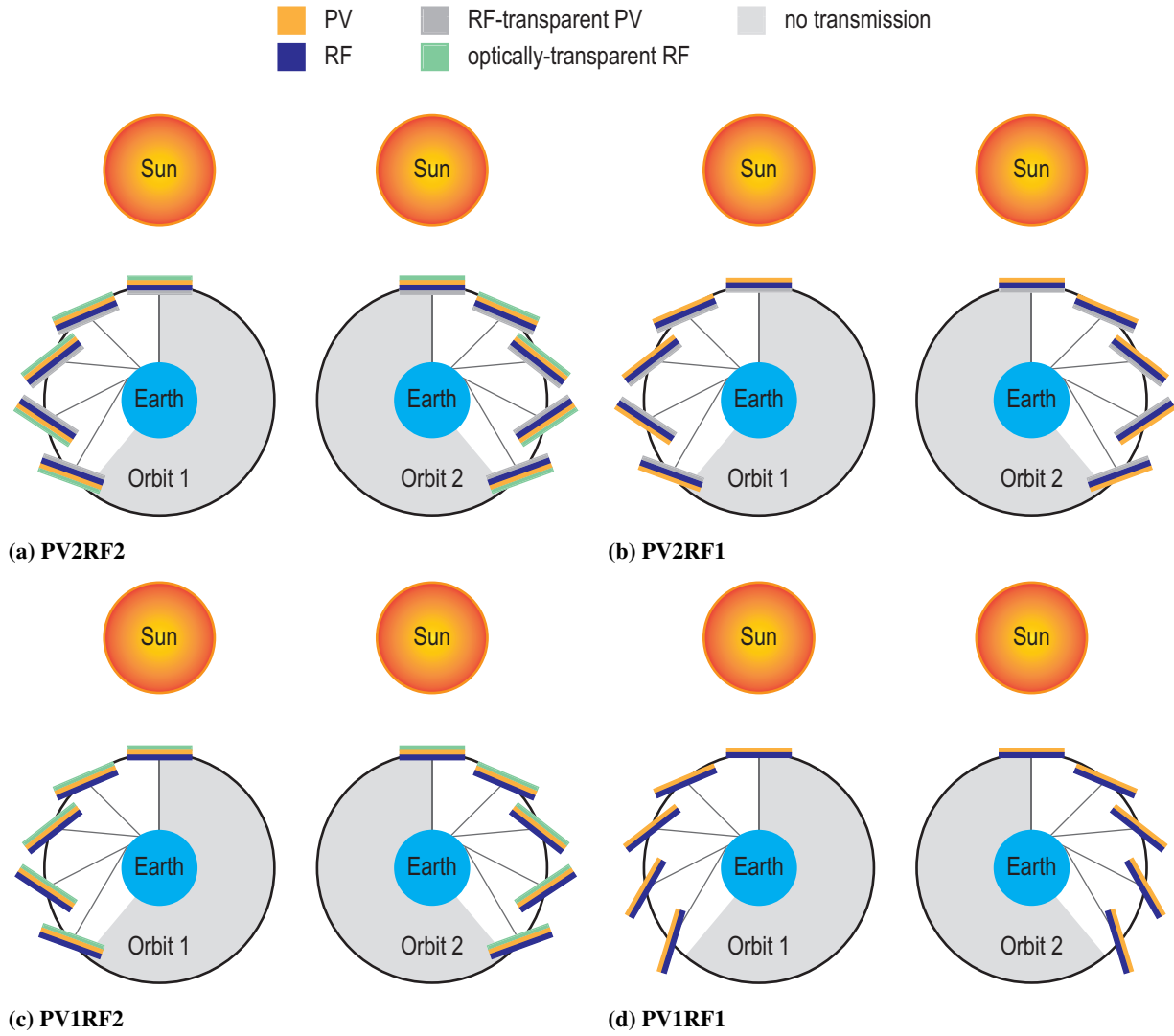
Fig. 18 Illustrations of the optimum orientations for single and dual-sided SSPSs in MEO. The shaded region of each orbit correspond to areas where the SSPS is below the horizon relative to the receiving station.

to the PV2RF1 solution.

An important observation from Figs. 19 and 20 is that the optimum orientations during each pass are very sensitive to the position of the SSPS relative to the receiving station. Figure 21 then shows that each dual-sided SSPS again realizes the same relative SSPS-Sun-receiving station geometry using a different combination of active PV and RF surfaces throughout the orbit. Conversely, the PV1RF1 solutions are distinct due to the corresponding pointing limitations.

Figures 19 and 21 also show that most but not all receiving station passes feature jumps. This is because there is a range of receiving station positions which never satisfy the jump conditions, Eq. (36). However, due to the short duration receiving station passes and the prevalence of jumps in LEO (typically one per pass), attitude dynamics considerations are expected to be a significant design driver for a LEO SSPS. In particular, a LEO SSPS requires larger attitude control torques and must slew faster than its MEO or GEO counterparts to execute these maneuvers.
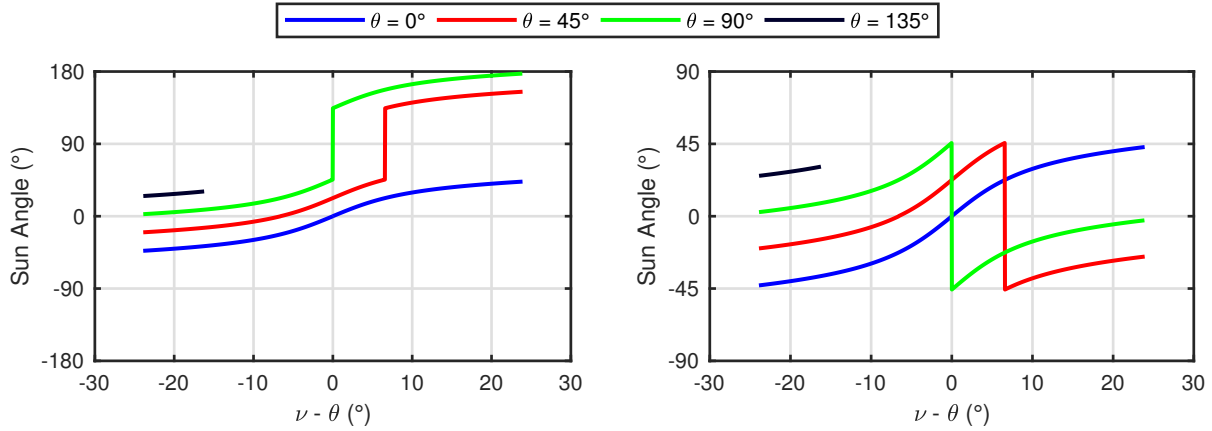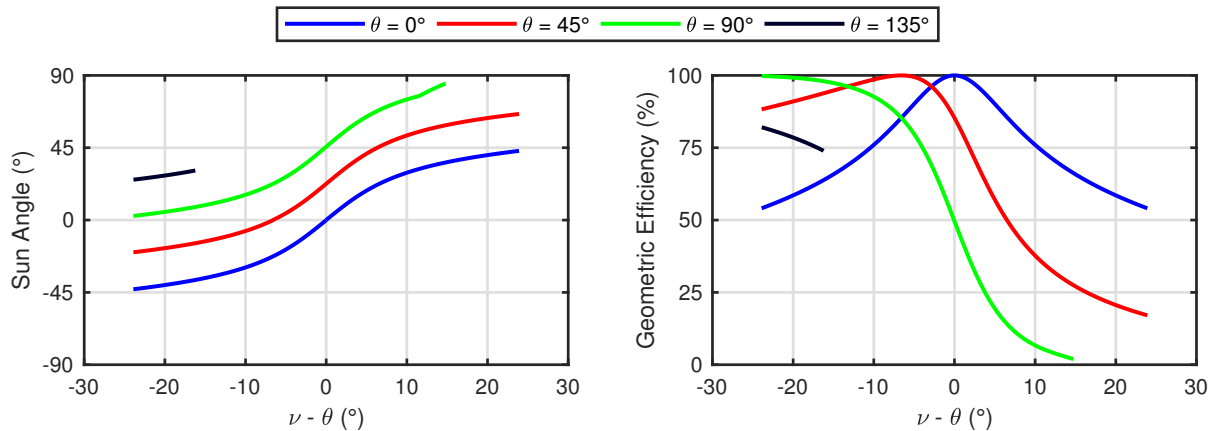
(a) Power-optimal attitude trajectories for PV2RF2 and PV2RF1 SSPSs.

(b) Power-optimal attitude trajectories for a PV1RF2 SSPS.
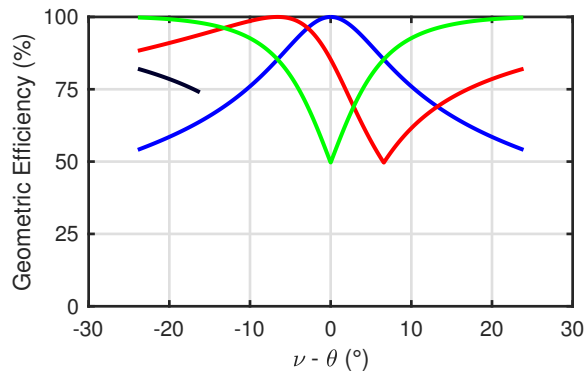

(c) Optimum geometric efficiency profiles.

Fig. 19 Solutions to the restricted power-optimal guidance problem for dual-sided SSPSs and inertially-fixed receiving stations located at $\theta = 0°, 45°, 90°$, and $135°$. For each pass, all three dual-sided SSPSs share the same optimum geometric efficiency depicted in (c).

(a) Power-optimal attitude trajectory.

(b) Optimum geometric efficiency profile.

Fig. 20 Solutions to the restricted power-optimal guidance problem for the PV1RF1 SSPS and inertially-fixed receiving stations located at $\theta = 0°, 45°, 90°$, and $135°$.
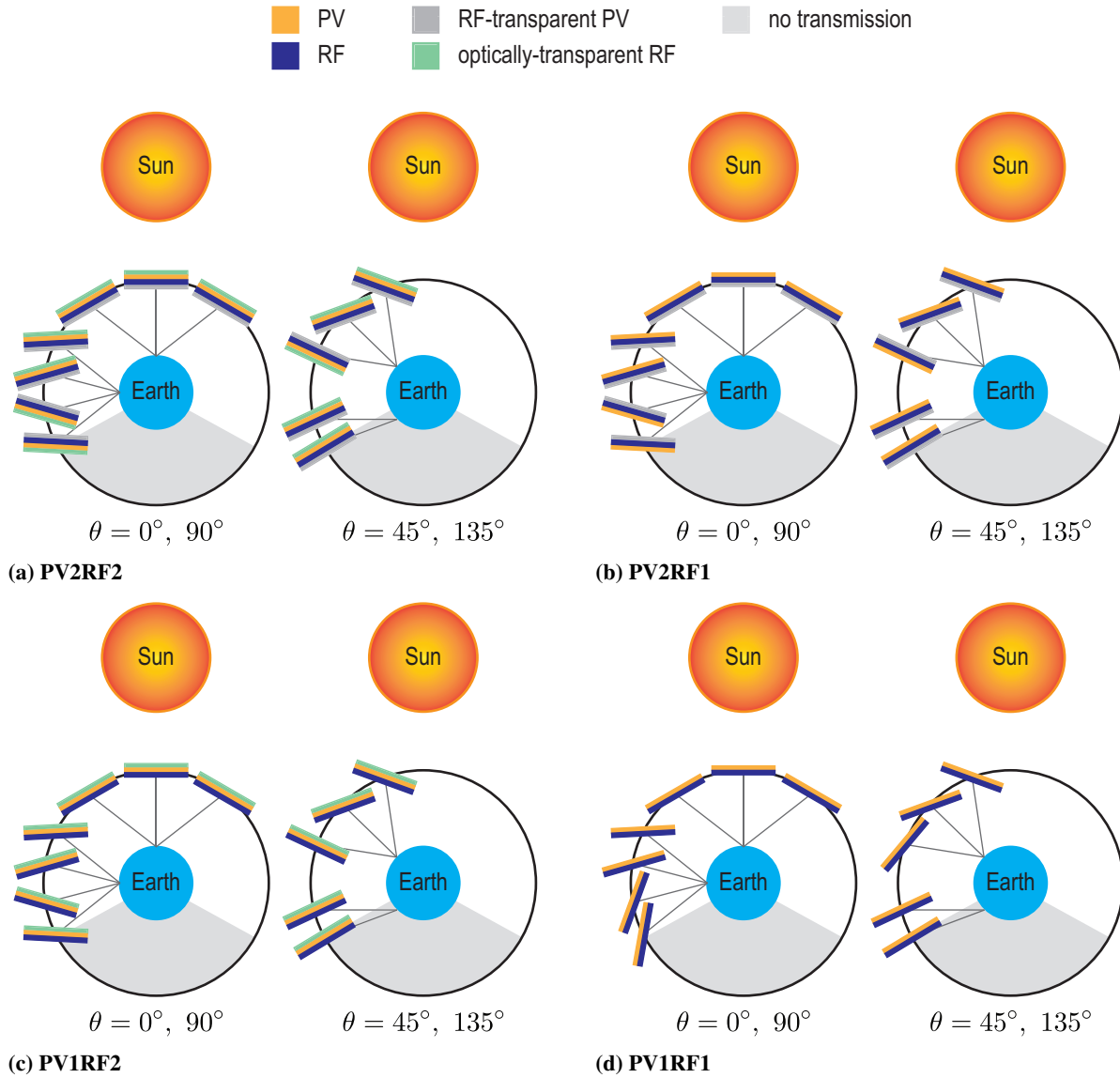
Fig. 21 **Illustrations of the optimum orientations for single and dual-sided SSPSs during receiving station passes at $\theta = 0°$, $45°$, $90°$, and $135°$ in LEO. Shaded regions correspond to the eclipse regions of each orbit.**

This section concludes by presenting the power-optimal guidance for an SSPS in an 881 km LEO during 14 orbits over the course of a sidereal day. Figure 22 depicts the elevation angles as a function of true anomaly. The orbit geometry is characterized by short duration receiving station passes that occur once per orbit. In this example, two of these passes (passes 7 and 8) occur when the SSPS is completely in eclipse. Another two passes (passes 6 and 9) predominantly occur in eclipse, although there are very short periods at the beginning of pass 6 and end of pass 9 where the SSPS is not in eclipse. Of the remaining ten passes, two are minimally affected by eclipsing. Due to these short duration passes and eclipsing, the solutions are undefined over a large percentage of each day. The elevation angle profiles for each pass are identical (aside from eclipse effects), but the SSPS orientation during each pass changes due to

differences in the SSPS-Sun-receiving station geometry.
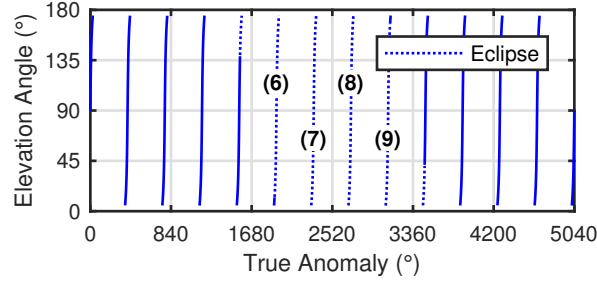
Fig. 22 Elevation angles for 14 orbits in LEO. Several passes are labeled with the number of their corresponding orbits.

Figure 23 depicts the dual-sided solutions for LEO. Due to the short duration receiving station passes, the LEO solutions are characterized by slow reconfiguration maneuvers that reorient the SSPS for the next receiving station pass. These reconfiguration maneuvers are represented by straight lines and occur when the SSPS is either in eclipse, below the horizon relative to the receiving station, or both.

Within each receiving station pass, the optimum orientations for the PV2RF2 and PV2RF1 SSPSs are physically the same. However, quantitative differences in the optimum orientations arise due to how the optimum orientations are connected between passes. In particular, the attitude of the SSPS is modulo 180°, whereas the attitude of a PV2RF1 SSPS is modulo 360°. This implies that a smaller angle change is often required to reorient a PV2RF2 SSPS for the next pass compared to a PV2RF1 SSPS. These differences are more easily highlighted by wrapping the PV2RF2 and PV2RF1 solutions to the domain $[-180°, 180°]$, as is done in Fig. 24.

Figure 25 then plots the PV1RF1 solution for LEO. Due to the short pass durations, the only substantial differences between the single and dual-sided solutions in LEO are the absence of jumps and the corresponding decrease in geometric efficiency.

Note that all four LEO solutions feature two kinks between $v = 1800°$ and $v = 3240°$. These kinks correspond to the portions of receiving station passes 6 and 9 from Fig. 22 that are not in eclipse.
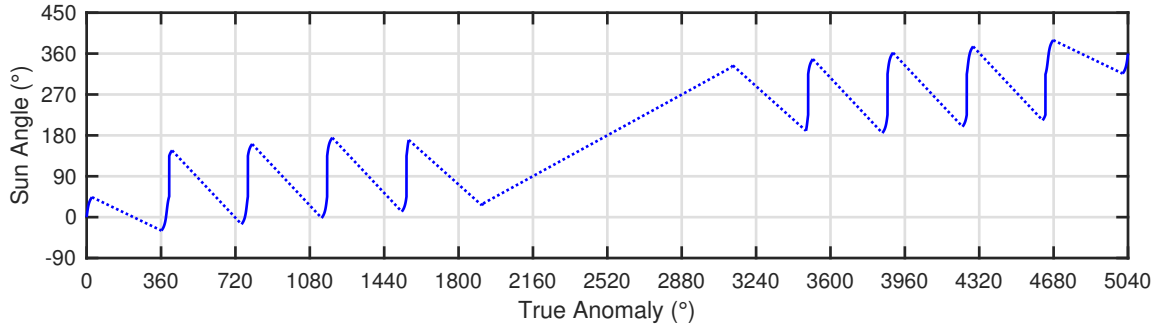
V. System Performance Metrics

Two metrics useful for comparing SSPS performance across a range of architectures and orbits are the day-averaged geometric efficiency, $\overline{G}$, and the received energy density (per unit receiver aperture area) per day, E_r. These performance metrics are defined as follows:

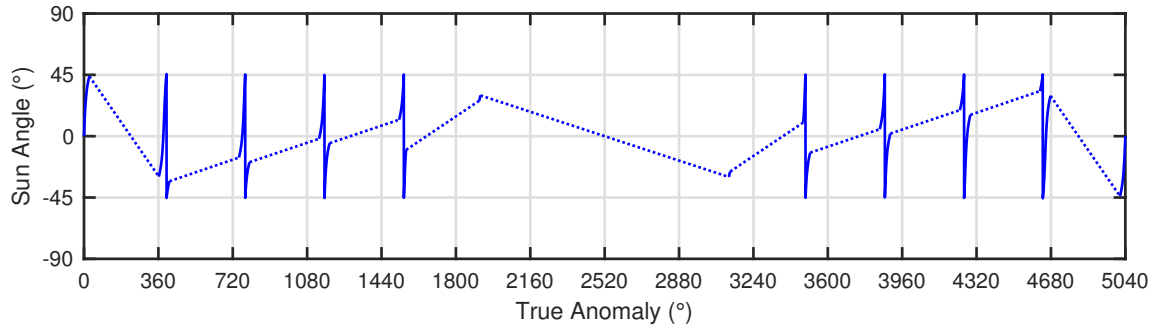$$\overline{G} = \frac{1}{t_f - t_0} \int_{t_0}^{t_f} G \, dt \tag{38}$$

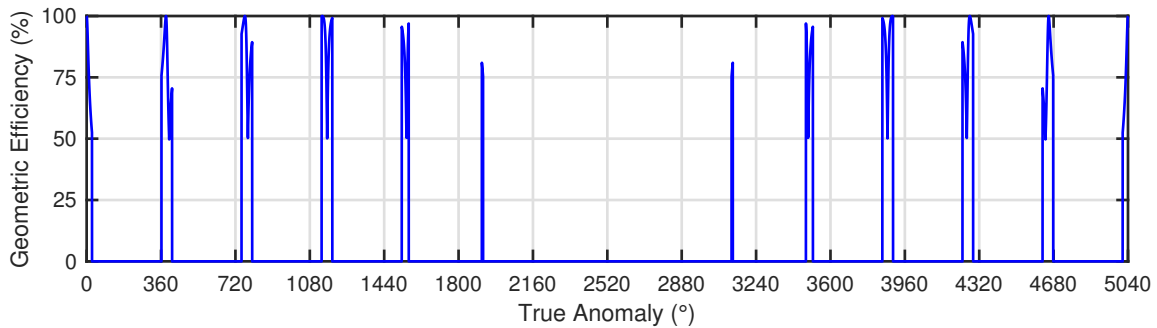$$E_r = \int_{t_0}^{t_f} W_r \, dt \tag{39}$$
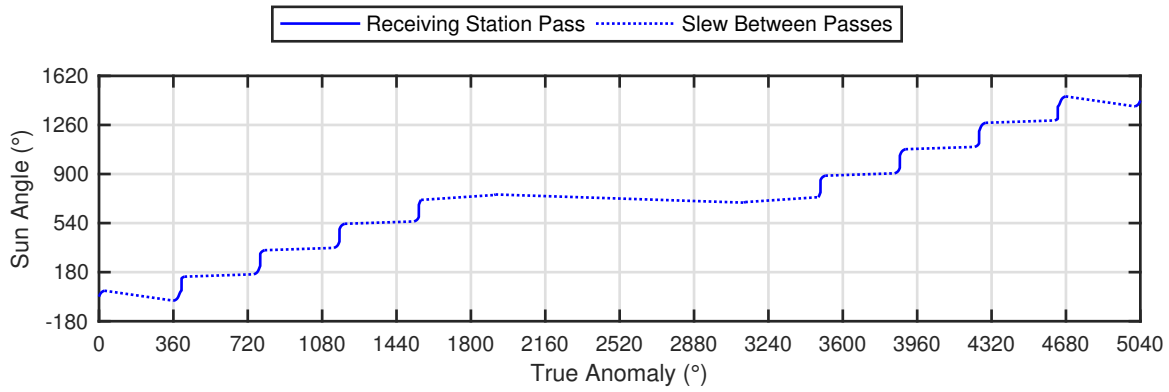
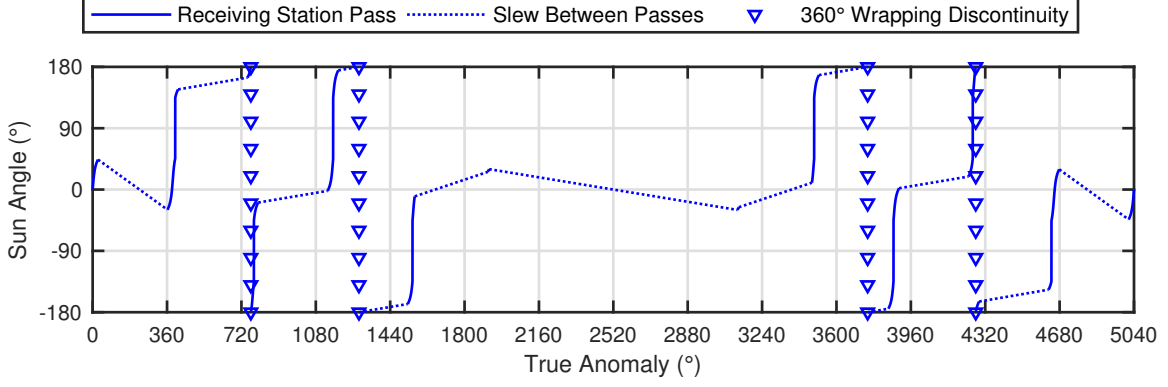(a) Trajectory for a PV2RF2 SSPS.

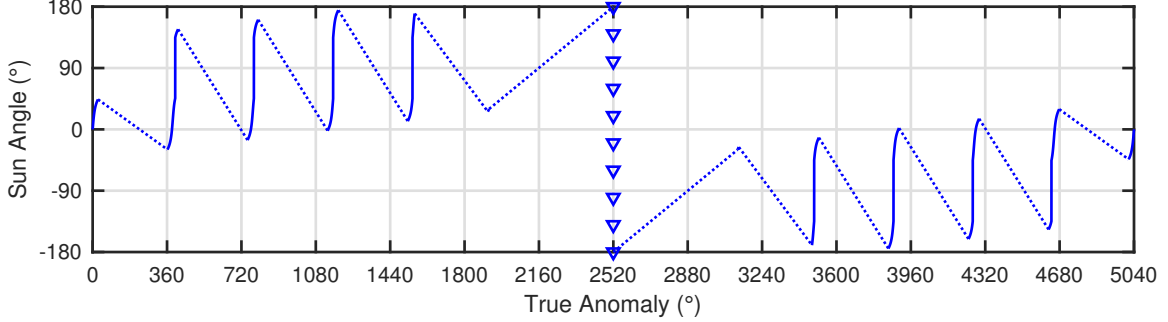(b) Trajectory for a PV2RF1 SSPS.

(c) Trajectory for a PV1RF2 SSPS.

(d) Optimum geometric efficiency profile for dual-sided SSPSs.

Fig. 23   Solutions to the restricted power-optimal guidance problem for dual-sided SSPSs for 14 orbits in LEO. All three dual-sided SSPSs share the same optimum geometric efficiency depicted in (d).

(a) Trajectory for a PV2RF2 SSPS.

(b) Trajectory for a PV2RF1 SSPS.

Fig. 24   Power-optimal attitude trajectories for PV2RF2 and PV2RF1 SSPSs in LEO wrapped to the domain [-180°,180°].

Again, only orbits that repeat an integer multiple of times per sidereal day are considered. Hence, t_0 and t_f coincide with the start and end of a sidereal day. By integrating over a sidereal day, $\overline{G}$ and E_r both account for receiving station access times and eclipse periods.

By averaging the transmitted power density, Eq. (18), over a sidereal day and using the definition of the geometric efficiency, Eq. (20), with Eq. (38), the transmitted energy density per day can be expressed as $E_t = \overline{W}_t \left(t_f - t_0 \right)$ where $\overline{W}_t$ is the average transmitted power density given by

$$\overline{W}_t = W_{\text{SF}} \, \eta_{\text{PV}} \, \eta_{\text{DC-RF}} \, \eta_{\text{Tx}} \, \overline{G} \tag{40}$$

The received power density in Eq. (39) is computed from a modified form of the Friis transmission equation [28]:

$$\frac{P_r}{P_t} = \eta_{\text{ML}} \frac{A_r A_t}{\rho^2 \lambda^2} \tag{41}$$

where $P_r = W_r A_r$, $P_t = W_t A_t$, η_{ML} is the percentage of the total radiated power contained in the main lobe of the RF beam, ρ is the slant range between the SSPS and receiving station, λ is the transmit wavelength, and W_t is given by
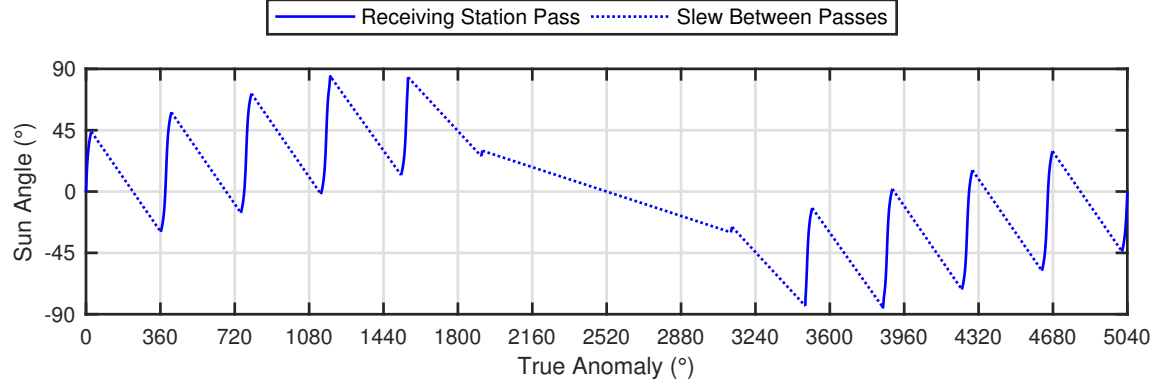
(a) Power-optimal attitude trajectory.
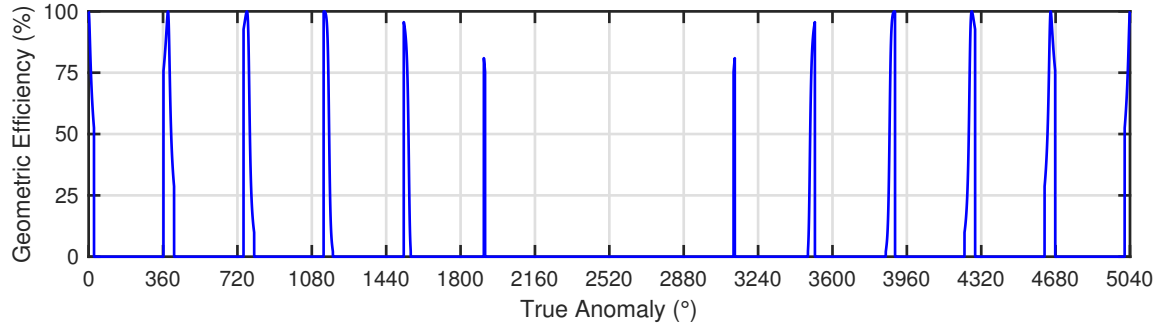
(b) Optimum geometric efficiency profile.

Fig. 25 Solution to the restricted power-optimal guidance problem for the PV1RF1 SSPS for 14 orbits in LEO.

Eq. (18). Rewriting Eq. (41) in terms of power densities then yields

$$W_r = \eta_{\mathrm{ML}} \frac{W_t A_t^2}{\rho^2 \lambda^2} \qquad (42)$$

which shows that the received power is strongly dependent on free space path losses ($1/\rho^2$ losses). Equation (42) neglects the increase in the size of the RF beam's footprint due to elevation angle effects. Elevation angle effects do not impact either the power transmitted or received so long as the receiving station is sized to capture the main lobe of the RF beam at the minimum elevation angle. However, larger receiving stations increase costs and are oversized for elevation angles that exceed the minimum elevation angle.

Only designs with transmit apertures that do not exceed the far-field limit of $\rho \gg 2A_t/\lambda$ [24] are considered, although it is possible to consider near-field designs with larger transmit apertures. In the far-field, an RF beam is approximately uniform with a well-defined main lobe. The main lobe is assumed to contain $\eta_{\mathrm{ML}} = 84\%$ of the total radiated power [29]. An efficient receiving station for a far-field system is designed to only capture the power transmitted in the main lobe, meaning that the optimum receiving station aperture size is a function of the transmit aperture size, the elevation angle, and the slant range between the SSPS and receiving station [30]. Requiring a system to operate in the far-field may restrict the aperture size, orbit altitude, or impose additional constraints on either elevation angle or squint

angle. For example, for an SSPS in a circular, 400 km orbit with a 10 GHz transmitter, the far-field assumption holds for square apertures with side lengths less than 77 m. This is especially important for non-geostationary orbits where the slant range depends on the elevation angle, meaning that the receiving station aperture must be sized for the orbit's minimum slant range. In contrast, the near-field radiation pattern for an RF beam is not uniform and strongly depends on the transmitter's characteristics. While it may be possible to design a ground segment for a near-field system that recovers more power than a far-field system with the same footprint, these considerations are outside the scope of this paper.

Figures 26 and 27 plot the day-averaged geometric efficiencies and energy densities for single and dual-sided SSPSs as a function of orbit altitude using the assumptions of the restricted power-optimal guidance problem. From the power-optimality theorem, all three dual-sided SSPSs share the same day-averaged geometric efficiencies, transmitted energy densities, and received energy densities. Figure 27 assumes a PV efficiency $\eta_{PV} = 25\%$, a DC-to-RF conversion efficiency $\eta_{DC\text{-}RF} = 33\%$, an antenna transmit efficiency $\eta_{Tx} = 95\%$, and a 10 GHz transmitter with an effective area of 625 m^2, corresponding to an SSPS with a 25 m $\times$ 25 m square aperture. Note that even though the received energy density scales with the square of the effective transmitter area, the trends in Fig. 27b are independent of aperture size.
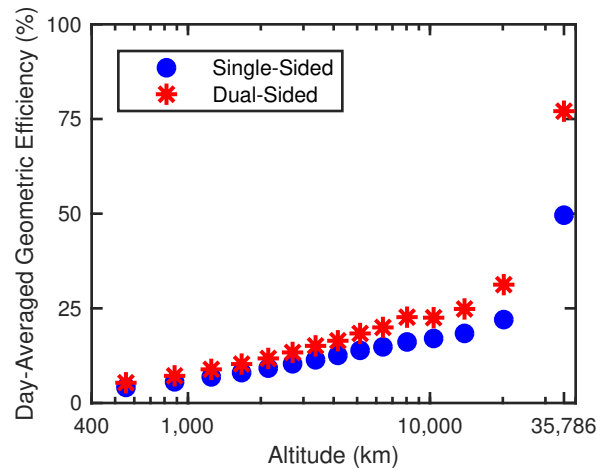
Fig. 26   Day-averaged geometric efficiencies for single and dual-sided SSPSs as a function of orbit altitude.

Several important trends are evident in Figs. 26 and 27. As predicted by the power-optimality theorem, dual-sided modules exhibit improved day-averaged geometric efficiencies relative to their single-sided counterparts, irrespective of altitude. However, both the day-averaged geometric efficiency and the performance advantage of a dual-sided module relative to a single-sided module decrease as the altitude decreases. Two factors drive these reductions: receiving station pass duration and eclipse duration. As the altitude decreases, the ground station pass duration decreases and the eclipse duration increases, leading to a net decrease in day-averaged geometric efficiency. Due to the PV1RF1 pointing constraints, eclipsing disproportionately affects dual-sided modules. In the absence of eclipse, a dual-sided module can transmit at any point in its orbit (so long as the receiving station is in view), unlike the PV1RF1 SSPS.

(a) Day-averaged transmitted energy density.   **(b) Day-averaged received energy density.**
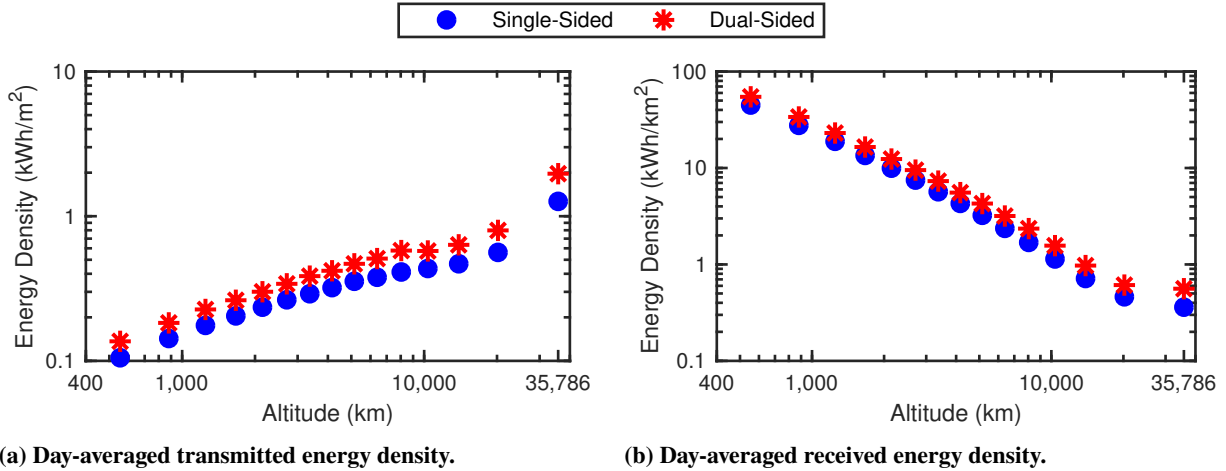
Fig. 27   Day-averaged transmitted and received energy densities for single and dual-sided SSPSs as a function of orbit altitude. Assumes an SSPS with a 625 m^2 aperture transmitting to a fixed-area receiving station. Note that transmitted and received energy densities are plotted using units of kWh/m^2 and kWh/km^2 to reflect the different length scales of the space and ground segments.

The corresponding decrease in transmitted energy density with decreasing altitude is depicted in Fig. 27a. However, Fig. 27b shows that the received energy density actually increases with decreasing altitude for a fixed-area receiver. This net increase in received energy is a consequence of reduced path losses. For a fixed-area receiving station, the reduction in path losses at lower altitudes outweighs the reduced day-averaged geometric efficiency.

However, Fig. 27 does not capture a critical disadvantage of non-geostationary orbits. Even though launching a system to LEO is cheaper than launching an equivalent system to GEO on a cost per kilogram basis, a single non-geostationary SSPS is only capable of providing intermittent power to any single location on Earth. Because receiving station pass duration decreases as altitude decreases, power becomes increasingly intermittent for SSPSs at lower altitudes. Even though the overall received energy density is higher in LEO, due to the finite number of receiving station passes, a constellation of multiple SSPSs or power storage solutions (e.g. batteries) are required to provide continuous power from an SSPS outside of GEO.

VI. Conclusion

This paper formulates the power-optimal guidance problem for a planar SSPS and solves the problem for the special case of an SSPS in a circular, equatorial orbit transmitting to an equatorial receiving station (the restricted power-optimal guidance problem). The power-optimal guidance problem arises because the orientations between the PV surface and the Sun and the RF surface and the receiving station are inherently coupled for a planar SSPS. Hence, the orientation that maximizes power collection is not necessarily the same as the orientation that maximizes power transmission.

Four distinct planar SSPS architectures were identified. Purely geometric arguments were used to demonstrate that having dual PV surfaces or dual RF surfaces significantly boosts the SSPS's performance relative to the baseline

PV1RF1 architecture. Under the assumptions of the restricted power-optimal guidance problem, a dual-sided SSPS can deliver over 50% more energy per orbit to the ground than a PV1RF1 SSPS for some orbits. The same geometric arguments were then used to prove that the power transmitted by a PV2RF2 SSPS is equivalent to the power transmitted by both PV2RF1 and PV1RF2 SSPSs. These results are independent of both the specific orbit and the characteristics of the PV cells and antennas for the restricted power-optimal guidance problem. However, implementing RF-transparent PV or optically-transparent RF are both extremely challenging technical problems. As a result, the mass, cost, and complexity penalties associated with designing and manufacturing dual PV surfaces or dual RF surfaces may outweigh the increase in system efficiency.

The restricted power-optimal guidance problem was then solved for an SSPS in GEO and representative medium and low Earth orbits. It was shown that as the orbit altitude decreases, the receiving station pass duration decreases and the eclipse duration increases, thereby resulting in a net decrease in system efficiency as the altitude decreases. In contrast, the average slant range between the SSPS decreases as the altitude decreases. As a result, for a fixed-area receiver, the received energy density actually increases as the altitude decreases. However, to increase the received energy density, the SSPS loses persistence because a single non-geostationary SSPS can only provide intermittent power to a single location.

Lastly, the power-optimal guidance solutions highlighted a key ramification of dual-sided operations, namely that the attitude trajectories that maximize power transmission are discontinuous and require instantaneous changes, or jumps, in the SSPS's orientation. Each jump reconfigures the SSPS by reducing the sun and squint angles relative to one set of PV and RF surfaces. Due to jumps, optimal attitude trajectories can only be followed approximately when attitude dynamics are included, thereby resulting in an efficiency loss. Hence, planarity couples the SSPS's efficiency to its attitude dynamics, making attitude dynamics a critical design driver for a planar SSPS.

Aside from considering non-circular and/or non-equatorial scenarios, the analysis can be extended to consider constellations or swarms of SSPSs. Additionally, consideration needs to be given to the numerous other GNC challenges, including orbit and attitude perturbations, attitude dynamics and control, and control-structure interactions, associated with realizing the ultimate goal of launching a space solar mission.

References

[1] Asimov, I., "Reason," *I, Robot*, 1941, pp. 59–77.

[2] Glaser, P. E., "Power from the Sun: Its Future," *Science*, Vol. 162, No. 3856, 1968, pp. 857–861. doi:10.1126/science.162.3856.857.

[3] Mankins, J. C., *The Case for Space Solar Power*, Virginia Edition Publishing, 2014.

[4] Carrington, C., Fikes, J., Gerry, M., Perkinson, D., Feingold, H., and Olds, J., "The Abacus/Reflector and integrated symmetrical concentrator - Concepts for space solar power collection and transmission," *35th Intersociety Energy Conversion Engineering Conference and Exhibit*, Las Vegas, Nevada, 2000, pp. 1–10. doi:10.2514/6.2000-3067.

[5] Mankins, J. C., "A Technical Overview of the "SunTower" Solar Power Satellite Concept," *Acta Astronautica*, Vol. 50, No. 6, 2002, pp. 369–377. doi:10.1016/S0094-5765(01)00167-9.

[6] Sasaki, S., Tanaka, K., Higuchi, K., Okuizumi, N., Kawasaki, S., Shinohara, N., Senda, K., and Ishimura, K., "A new concept of solar power satellite: Tethered-SPS," *Acta Astronautica*, Vol. 60, No. 3, 2007, pp. 153–165. doi:10.1016/j.actaastro.2006.07.010.

[7] Li, Q., Deng, Z., Zhang, K., and Wang, B., "Precise Attitude Control of Multirotary-Joint Solar-Power Satellite," *Journal of Guidance, Control, and Dynamics*, Vol. 41, No. 6, 2018, pp. 1435–1442. doi:10.2514/1.G003309.

[8] Arya, M., Lee, N., and Pellegrino, S., "Ultralight Structures for Space Solar Power Satellites," *3rd AIAA Spacecraft Structures Conference*, San Diego, California, 2016, pp. 1–18. doi:10.2514/6.2016-1950.

[9] Jaffe, P., and McSpadden, J., "Energy Conversion and Transmission Modules for Space Solar Power," *Proceedings of the IEEE*, Vol. 101, No. 6, 2013, pp. 1424–1437. doi:10.1109/JPROC.2013.2252591.

[10] Gdoutos, E. E., Leclerc, C., Royer, F., Kelzenberg, M. D., Warmann, E. C., Espinet-Gonzalez, P., Vaidya, N., Bohn, F., Abiri, B., Hashemi, M. R., Gal-Katziri, M., Fikes, A., Atwater, H., Hajimiri, A., and Pellegrino, S., "A Lightweight Tile Structure Integrating Photovoltaic Conversion and RF Power Transfer for Space Solar Power Applications," *2018 AIAA Spacecraft Structures Conference*, Kissimmee, Florida, 2018, pp. 1–12. doi:10.2514/6.2018-2202.

[11] Mankins, J. C., "A fresh look at space solar power: New architectures, concepts and technologies," *Acta Astronautica*, Vol. 41, No. 4, 1997, pp. 347–359. doi:10.1016/S0094-5765(98)00075-7.

[12] Wie, B., and Roithmayr, C., "Integrated orbit, attitude, and structural control system design for space solar power satellites," *AIAA Guidance, Navigation, and Control Conference and Exhibit*, Montreal, Canada, 2001, pp. 1–11. doi:10.2514/6.2001-4273.

[13] Wie, B., and Roithmayr, C. M., "Attitude and Orbit Control of a Very Large Geostationary Solar Power Satellite," *Journal of Guidance, Control, and Dynamics*, Vol. 28, No. 3, 2005, pp. 439–451. doi:10.2514/1.6813.

[14] McNally, I. J., Scheeres, D. J., and Radice, G., "Attitude Dynamics of Large Geosynchronous Solar Power Satellites," *AIAA/AAS Astrodynamics Specialist Conference, AIAA SPACE Forum*, San Diego, California, 2014, pp. 1–13. doi:10.2514/6.2014-4123.

[15] Wu, S., Zhang, K., Peng, H., Wu, Z., and Radice, G., "Robust optimal sun-pointing control of a large solar power satellite," *Acta Astronautica*, Vol. 127, 2016, pp. 226–234. doi:10.1016/j.actaastro.2016.05.019.

[16] Goel, A., Lee, N., and Pellegrino, S., "Trajectory design of formation flying constellation for space-based solar power," *2017 IEEE Aerospace Conference*, Big Sky, Montana, 2017, pp. 1–11. doi:10.1109/AERO.2017.7943711.

[17] Goel, A., Chung, S.-J., and Pellegrino, S., "Trajectory Design of a Spacecraft Formation for Space-Based Solar Power Using Sequential Convex Programming," *Proceedings of the 9th International Workshop on Satellites Constellations and Formation Flying (IWSCFF)*, Boulder, Colorado, 2017, pp. 1–20.

[18] R. Ortizlongo, C., and L. Rickman, S., "Method for the Calculation of Spacecraft Umbra and Penumbra Shadow Terminator Points," Tech. Rep. NASA-TP-3547, NASA, Lyndon B. Johnson Space Center, Houston, Texas, April 1995.

[19] Mello, S. F., "Analytical study of the Earth's shadowing effects on satellite orbits," *Celestial Mechanics and Dynamical Astronomy*, Vol. 5, No. 1, 1972, pp. 80–101. doi:10.1007/BF01227825.

[20] McMahon, J. W., and Scheeres, D. J., "New Solar Radiation Pressure Force Model for Navigation," *Journal of Guidance, Control, and Dynamics*, Vol. 33, No. 5, 2010, pp. 1418–1428. doi:10.2514/1.48434.

[21] Früh, C., Kelecy, T. M., and Jah, M. K., "Coupled orbit-attitude dynamics of high area-to-mass ratio (HAMR) objects: influence of solar radiation pressure, Earth's shadow and the visibility in light curves," *Celestial Mechanics and Dynamical Astronomy*, Vol. 117, 2013, pp. 385–404. doi:10.1007/s10569-013-9516-5.

[22] Bate, R. R., Mueller, D. D., and White, J. E., *Fundamentals of Astrodynamics*, Dover Publications, Inc., New York, 1971, Chap. 4.

[23] Escobal, P. R., *Methods of Orbit Determination*, 2nd ed., Krieger Publishing Company, Inc., Malabar, Florida, 1976, Chap. 4.

[24] Balanis, C. A., *Antenna Theory: Analysis and Design*, 3rd ed., John Wiley & Sons, Inc., Hoboken, New Jersey, 2005.

[25] Strang, G., *Calculus*, Wellesley-Cambridge Press, Wellesley, MA, 1991, Chap. 2, p. 89.

[26] Larson, W. J., and Wertz, J. R., *Space Mission Analysis and Design*, 3rd ed., Microcosm Press and Kluwer Academic Publishers, El Segundo, California and Dordrecht, The Netherlands, 1999, Chap. 8, pp. 203–240.

[27] Press, W. H., Flannery, B. P., Teukolsky, S. A., and Vetterling, W. T., *Numerical Recipes in C: The Art of Scientific Computing*, 2nd ed., Cambridge University Press, New York, 1992, Chap. 10, pp. 397–402.

[28] Friis, H. T., "A Note on a Simple Transmission Formula," *Proceedings of the IRE*, Vol. 34, No. 5, 1946, pp. 254–256. doi:10.1109/JRPROC.1946.234568.

[29] Hecht, E., *Optics*, 3rd ed., Addison-Wesley Longman, Boston, Massachusetts, 1997.

[30] Jelalian, A. V., *Laser Radar Systems*, Artech House, Boston, Massachusetts, 1991.